An Experimental Examination of the Effect of Trailing Edge Injection on the Aerodynamic Performance of Gas Turbine Blades

by

Richard Tompkins Singer, Jr.

Thesis submitted to the Faculty of the

Virginia Polytechnic Institute and State University

in partial fulfillment of the requirements for the degree of

Master of Science

in

Mechanical Engineering

APPROVED:

_____
Dr. Hal L. Moses, Chairman

_____   _____
Dr. Wing F. Ng   Dr. Thomas E. Diller

December 16, 1988

Blacksburg, Virginia

An Experimental Examination of the Effect of Trailing Edge Injection on the Aerodynamic Performance of Gas Turbine Blades

by

Richard Tompkins Singer, Jr.

Dr. Hal L. Moses, Chairman

Mechanical Engineering

(ABSTRACT)

This thesis documents an experimental investigation into the effect of trailing edge injection on the aerodynamic performance of turbine blades conducted at Virginia Polytechnic Institute and State University (VPI&SU). A brief description of the arrangement, instrumentation and data acquisition system of the VPI&SU Transonic Cascade Wind Tunnel is given. Testing was conducted under a number of test conditions. Baseline data was obtained for the blades with no trailing edge injection. The blades were then tested for two different blowing rates to test the effect of blowing rate on the total pressure loss coefficient, $\bar{L}$. Tests were conducted at a variety of save cascade exit Mach numbers ranging from 0.79 to 1.36. Measurements were taken at three locations downstream of the cascade blade trailing edges. The algorithm used to calculate the $\bar{L}$ from the measured data is discussed. Results of the testing indicate that trailing edge injection has a negligible effect on the total pressure loss coefficient. Correlations of cascade exit Mach number to $\bar{L}$ are given. The development of $\bar{L}$ downstream of the blade trailing edge is discussed.

Acknowledgements

A project such as the one described in this thesis cannot be successfully completed without the help of a great many people. Thanks to General Electric Company, Aircraft Engine Business for providing funding for this project. I am especially grateful to Mr. Brent Gregory of GE for his personal involvement and many contributions. I would also like to thank Dr. W. F. Ng and Dr. T. E. Diller for serving as members of my thesis committee and for providing constructive criticism of this work.

One person without whom this project would never have been completed is His hard work and sense of humor made what was sometimes a difficult job a good deal easier. It would be a grave omission to forget to thank all of the men in the Mechanical Engineering machine shop who kept this project going from the mechanical end. I owe a special debt of gratitude to a skilled machinist, and seemingly possessed of inexhaustible patience for a graduate student relatively ignorant in the requirements of the machining process. He performed more jobs that I needed "yesterday" than I ever should have had the gall to request.

Final thanks go to my advisor, Dr. Hal L. Moses. In addition to the subjects I learned from him in classes, his answers to a great many questions posed by me have significantly

contributed to my understanding, such as it is, of the science of fluid mechanics. My successful completion of this thesis and my Master's degree are due in no small part to his guidance, for which I will always be grateful.

It is impossible to mention everyone who contributed to this work, so I hope this general statement of gratitude will suffice. The one person to whom I owe the most, though she took no part in this project, is my wife   She encouraged me to undertake graduate work in the first place, and she supported me when the going was less than smooth. Her love and understanding are the most important things in my life and this work would never have been completed without them.

Table of Contents

List of Illustrations

List of Tables

List of Symbols

$\eta_{th,max}$ = Carnot efficiency

T_H = temperature of high temperature reservoir in Carnot cycle

T_L = temperature of low temperature reservoir in Carnot cycle

$T_{t,i}$ = turbine inlet temperature

Δp_t = total pressure loss

p = static pressure

p_t = total pressure

P_t = reduced total pressure loss

$\overline{L}$ = mass averaged total pressure loss coefficient

B = blowing rate

$\dfrac{A}{A^*}$ = critical area ratio

$M_{2,isen}$ = isentropic Mach number downstream of blade row

$\dfrac{x}{c}$ = nondimensional x-coordinate based on blade chord

$p_{t,2,prb}$ = total pressure downstream of cascade measured by total pressure probe

M_x = Mach number upstream of normal shock

$p_{t,x}$ = total pressure upstream of normal shock

M_y = Mach number downstream of normal shock

$p_{t,y}$ = total pressure downstream of normal shock

γ = ratio of specific heats

ρ = density of fluid

V = velocity of fluid

u = velocity of fluid normal to direction of integration

R = universal gas constant

y_p = position of the total pressure probe

δy = change in position of total pressure probe between measurement points

β_1 = inlet flow angle

β_2 = exit flow angle

c = blade chord

s = blade spacing

h = blade width (span)

T_t = total temperature

T = static temperature

$M_{2,isen,avg}$ = average value of isentropic Mach number downstream of the blade row for a group of data taken with the same tailboard setting.

U = uncertainty

b = bias

t_{95} = statistical parameter, set equal to 2.0

S = precision index

Subscripts

1 = upstream of blade row

2 = downstream of blade row

c = coolant stream

o = main stream

b,s = suction surface of blade

b,p = pressure surface of blade

w,f = cascade wall, forward measurement location

w,r = cascade wall, rear measurement location

Abbreviations

VPI&SU = Virginia Polytechnic Institute and State University

1.0   Introduction

Since 1939, when the first gas turbine was employed for aircraft propulsion, there has been a constant effort to improve their efficiency. To this end, each component has been scrutinized for ways to improve it's performance so that the overall gas turbine efficiency is increased. By virtue of extensive development, the aerodynamic efficiencies in the range of 90 percent achieved by modern turbines and compressors is considered to be close to the maximum, especially from a cost/benefit point of view. The same is true for the combustor and gas flow passages.

In order to cope with ever-present demands for more effective machines, gas turbine designers have two obvious alternatives to pursue. The first option is to reduce the weight of the machine without sacrificing performance. This may be achieved by the use of exotic, lightweight alloys and composites and advanced manufacturing processes. While the potential for gains in efficiency as a result of reducing the weight of the machine provides compelling motivation for research, the technical obstacles presented by the use of these materials and processes has limited their practical application thus far.

Another avenue gas turbine designers have pursued is revealed by an analysis of the thermodynamics of the gas turbine. An analysis of the Carnot cycle is helpful in determining

how the thermal efficiency of the gas turbine may be maximized. The Carnot efficiency is, of course, the maximum efficiency achievable by any real heat engine. Following van Wylen and Sonntag [1] the efficiency of a Carnot cycle, operating between a high temperature reservoir at temperature T_H and a low temperature reservoir at temperature T_L, is given as

$$\eta_{th,max} = 1 - \frac{T_L}{T_H} \quad [1.1]$$

It is obvious from this relation that $\eta_{th,max}$ may be increased by lowering T_L or raising T_H. In the case of an aircraft gas turbine, the atmosphere is considered as the low temperature reservoir, and as such its temperature is not subject to direct control, except by varying flight altitude. Therefore, the temperature of the high temperature reservoir must be increased to raise $\eta_{th,max}$.

For a real gas turbine, T_H corresponds to the temperature at the outlet of the combustor, the so-called turbine inlet temperature, $T_{t,i}$. As gas turbine design progressed and $T_{t,i}$ was raised to achieve higher and higher efficiencies, the gas turbine designers were restricted by the temperature limits of the materials used in the machines. Turbine blades, with their position directly in the flow path of hot gases and thin trailing edges, are especially vulnerable to high temperature failure mechanisms such as creep and outright melting.

The solution to this problem has several parts. Turbine blades made of high temperature materials such as ceramics may be effective in the future, but their material properties are such that further development is required before they can be used in practice. Another course of action being pursued is to reduce the operating temperature of the turbine blades by actively cooling them. This involves supplying coolant, usually air taken from the gas turbine compressor, to the ends of the blades and exhausting the coolant into the main flow through holes in the surfaces of the blades. Cooling of the turbine blade surfaces is commonly achieved two ways. One way is to rely on convective cooling where heat is transferred from

the blade surfaces to coolant flowing in internal passages in the blades which is then exhausted into the main turbine flow through holes near the trailing edge of the blade. This method is referred to as *trailing edge injection*. The other method is to exhaust the coolant out of rows of holes at the leading edge of the blades and (usually) additional rows of holes in the suction and pressure surfaces further back in the flow direction. The exhausted coolant spreads out in a thin layer over the blade surfaces providing insulation from the hot temperatures in the main flow in addition to cooling by convection. This method is referred to as *film cooling*. It should be noted that increasing the overall efficiency by raising $T_{t,i}$ can have negative effects. Diverting a portion of the compressor flow and using it for turbine blade cooling causes a decrease in the overall gas turbine efficiency. This effect will partially offset the increase in efficiency resulting from an increase in $T_{t,i}$. As a larger percentage of the compressor flow is diverted, this offsetting effect increases proportionately. Clearly then, raising $T_{t,i}$ to achieve higher efficiencies will eventually require a high enough cooling air flow that that these efficiency gains will be negated.

While the turbine blade cooling schemes discussed above are effective in allowing gas turbines to operate at higher values of $T_{t,i}$, they also present a potential problem. Injection of the coolant into the main flow of the turbine, with the attendant thickening of the blade trailing edges, could affect the aerodynamics of the airfoils. Specifically, the coolant injection could increase the aerodynamic losses of the airfoils through boundary layer thickening, adverse shock/boundary layer interaction or a number of unforseen fluid mechanics effects.

An experimental investigation of the effects of trailing edge injection on the aerodynamic performance of gas turbine blades forms the basis of the research documented by this thesis. In practice, a combination of film cooling and trailing edge injection is used. While this arrangement provides a higher degree of cooling than would either method used individually, the combination of the film cooling and trailing edge injection serves to complicate the fluid mechanics involved. In order to simplify the problem for study, this research investigates the effects of trailing edge injection only.

This thesis will provide the results of the research discussed above. Nomenclature will be introduced by which the aerodynamic performance of airfoils may be quantified, both with measured and calculated parameters. A description of the arrangement of the experiment and the testing program is provided. The results of the research and the conclusions drawn from the results are discussed. Finally, an uncertainty analysis to quantify the accuracy of the data will be provided.

2.0 Literature Review

This chapter is included in order to summarize information available in the literature which is relevant to the present research. The areas in which literature is cited are: general references for cascade testing, trailing edge injection research and development of experimental pressure loss correlations.

2.1 General References

The research documented by this thesis is a continuation of the work started by Zaccaria [2]. In his thesis, Zaccaria describes the development of the VPI&SU Transonic Cascade Wind Tunnel, and preliminary research investigating the periodicity of the flow in the cascade. Special emphasis was placed on minimizing the shock reflections off of the back wall of the test section and back into the flow. These reflections contribute to flow non-uniformity among the blade passages in the cascade. A variety of tailboard configurations, including solid and porous tailboards, and the use of no tailboard are recommended in the literature. Zaccaria concluded that the porous tailboard offered no advantage over the solid

tailboard in terms of preventing or reducing the strength of shock reflections. The solid tailboard was found to cause the cascade exit Mach number to be independent of the cascade inlet total pressure. Considering the diversity of recommended tailboard arrangements in the literature cited by Zaccaria, one may conclude that results of cascade testing is facility-dependent to some degree. This conclusion is supported by the study conducted by Kiock, et al. [3], which documented the testing of the same blade profile in four different tunnels. This study notes some variation of results between tunnels, especially loss coefficient at exit Mach numbers in the range from 1 to 1.3.

Zaccaria's thesis includes a summary of the literature concerning cascade testing in general, particularly transonic cascade testing. Works by Oates [4] and Gostelow [5] are also appropriate as general references for information on cascade testing.

2.2 Trailing Edge Injection Research

As stated in Chapter 1.0, the effect of trailing edge injection on turbine blade losses were of particular interest during this research. The literature is somewhat limited on this topic, and results available thus far are inconclusive. For the results available in the literature, several injection hole configurations were tested, the majority being the fluid passing directly out of the blade trailing edge. This geometry is used by some engine manufacturers and is suitable for fundamental study of the physics of trailing edge injection. However, the thick trailing edges required by such a configuration serve to magnify the pressure losses of turbine blades, especially with low blowing rates. MacMartin and Norbury [6] and others suggest that the total pressure loss of a transonic turbine blade is strongly influenced by the thickness of the trailing edge.

Venediktov [7] investigated the effect of trailing edge injection using four different injection hole configurations. The geometries studied include holes directly through the trailing edge, holes in the suction and pressure surfaces near the trailing edge, and holes at the trailing edge of a geometry similar to that shown in Figure 14. Experiments were conducted with exit Mach numbers in the range from 0.5 to 1.1 with injection mass flow ratios up to 7 percent. Venediktov concluded that, with appropriately sized injection holes, trailing edge injection had negligible effect on the blade efficiency.

As was referred to earlier, MacMartin and Norbury [6] conducted an investigation of the aerodynamics of a turbine cascade with trailing edge injection. The blades used in this study had relatively thick trailing edges due to the injection holes passing directly through the trailing edge. The exit Mach number was approximately 1.25, and the injection mass flow ratio ranged up to 7 percent. The authors of this research also concluded that trailing edge injection had little effect on the total pressure loss.

Lawaczeck [8] also conducted an investigation into the influence of trailing edge injection on the aerodynamic data from a transonic turbine cascade. As was the case with the research discussed above, the test blades had injection holes which passed directly through the trailing edge, with the associated relatively thick trailing edges. The exit Mach numbers tested ranged from 0.5 to 1.4, and injection flow ratios up to 4 percent were tested. Lawaczeck concluded that trailing edge injection does have an appreciable effect on the aerodynamics of the turbine blade tested. It should be noted that at transonic and supersonic exit Mach numbers, the blades were not operating under design conditions as evidenced by the severe suction surface separation noted by the author. Thus the results obtained from this experiment are somewhat inconclusive.

Finally, Xu and Denton [9], while investigating the relationship between trailing edge injection and base pressure, also examined the effect of trailing edge injection on total pressure loss. Measurements were made with exit Mach numbers of 0.9 and 1.15. The injection

mass flow ratio was approximately 1 percent. The results were inconclusive as to the effect of trailing edge injection on total pressure loss; however, a significant increase in base pressure was noted. This result confirms the earlier finding of Sieverding [10].

2.3 Experimental Pressure Loss Correlations

According to Kacker and Okapuu [11], a number of loss correlations have been developed, the most widely used being that described by Ainley and Matheson [12]. Kacker and Okapuu continue that the original correlation was refined by Dunham and Came [13]. Kacker and Okapuu show that a lack of experimental transonic cascade data renders previous loss correlations unreliable. The so-called AMDC loss correlation is shown to overestimate total pressure loss significantly at exit Mach numbers greater than one and the Kacker/Okapuu refinement is shown to improve correlation to experimental data. It is noted that neither correlation incorporates the effects of trailing edge injection.

3.0 Discussion

3.1 Introduction of Nomenclature

This section is included to define some terms which will be used throughout this thesis. .

3.1.1 Total Pressure Loss Coefficient

The stated purpose of the research documented by this thesis is to examine the effect of trailing edge injection on the aerodynamic performance of gas turbine blades. This section is provided to introduce terms which are used to quantify the *aerodynamic performance* of gas turbine blades. One measure of the aerodynamic performance of turbine blades is the decrease in total pressure as the fluid flows through the blade passages. A blade passage consists of the pressure surface of one blade and the suction surface of an adjacent blade (Figure 1). The total pressure loss across a blade row, Δp_t is given as

$$\Delta p_t = p_{t,1} - p_{t,2} \quad [3.1]$$

where $p_{t,1}$ and $p_{t,2}$ are the total pressure upstream and downstream of the blade row, respectively. This quantity may be ratioed with $p_{t,1}$ to give a nondimensional parameter P_t. Hence

$$P_t = \frac{(p_{t,1} - p_{t,2})}{p_{t,1}} = \frac{\Delta p_t}{p_{t,1}} \quad [3.2]$$

P_t may be interpreted as the percentage of the total pressure upstream of the blades that is lost as the fluid flows through the blade passages. Since the total pressure would remain constant if the flow were isentropic, P_t correlates to the fluid losses due to viscosity, compressibility, and in the case of coolant injection, mixing losses.

Following Oates [4], the entire loss for one blade is calculated by integrating P_t over one blade spacing (Figure 2). The effects of velocity variation in the direction of integration are accounted for by mass flow averaging. In this way, losses which occur in regions of high flow rate are weighted more than equivalent losses which occur in regions of low flow rate. Thus, the mass-averaged total pressure loss coefficient, $\bar{L}$ is given as

$$\bar{L} = \frac{\int_0^l \rho u P_t \, dy}{\int_0^l \rho u \, dy} \quad [3.3]$$

Note that $\bar{L}$ is related to the often used total pressure loss coefficient Y as follows:

$$Y = \frac{\Delta p_t}{p_{t,1} - p_2} = P_t \frac{p_{t,1}}{p_{t,1} - p_2}$$

3.1.2 Blowing Rate

The main goal of the research is to examine the cause and effect relationship between trailing edge injection and the aerodynamic performance of turbine blades. In order to establish this relationship, measurements were made with different amounts of trailing edge injection. In order to characterize the *amount* of trailing edge injection, a parameter used by Haller and Camus [14] called the blowing rate, B, is introduced. The blowing rate is defined as

$$B = \frac{(\rho_c V_c)}{(\rho_o V_o)} \quad [3.4]$$

where the density and velocity of both the coolant flow and the main flow are based on conditions at the point of injection.

3.2 Description of the Experiment

This section provides a description of the equipment used to conduct the research and the actual test program that was carried out. The physical arrangement of the apparatus used, including the wind tunnel itself, the coolant injection system, and the instrumentation, will be discussed. A description of the parameters measured and the various testing conditions examined is given.

3.2.1 Arrangement of Apparatus

3.2.1.1 Wind Tunnel

The wind tunnel used to conduct the research described herein is shown schematically in Figure 3 and Figure 4. It is a blowdown type wind tunnel supplied by storage tanks which are pressurized by four reciprocating compressors. Controlling the air flow from the storage tanks to the wind tunnel is a pneumatic valve which acts both as a shut-off valve and a flow regulating valve. The wind tunnel itself is composed of 14 in, Schedule 30 (35.56 cm OD/33.65 cm ID) carbon steel pipe with an integral flow straightener and the test section.

Control Valve Operating System

The control valve operating system (Figure 5) consists of an electronic control circuit, an electro-pneumatic converter, a valve actuating air supply and a constant reference pressure source. It is employed to control the operation of the valve over time so that air is supplied to the test section at a desired flow rate that is held as constant as possible while data is being recorded. When the storage tanks are pressurized, a pressure transducer measures the pressure in the tanks. The transducer output voltage is fed to the valve control circuit where it produces a proportionate output voltage which is applied to the electro-pneumatic converter. The electro-pneumatic converter is an adjustable pressure regulator, the degree of pressure reduction being related to the voltage applied to it. The inlet pressure to the electro-pneumatic converter is supplied by the constant reference pressure source. The output pressure of the electro-pneumatic converter is applied to the control valve actuator. When the full reference pressure is applied to the control valve actuator, the valve is fully opened. As the reference pressure is reduced by the electro-pneumatic converter the valve closes proportionately. Thus, the valve control circuit output voltage is converted to a corresponding control valve opening via the electro-pneumatic converter. As the pressure in the storage

tanks falls during operation of the wind tunnel, the valve control circuit output voltage (and the control valve opening) change accordingly. The valve control circuit output voltage has two adjustments. One is an offset to the storage tank pressure transducer output signal. By adjusting this offset, the amount of opening (and thus the air flow rate) when the valve is initially opened is set to the desired level. The other adjustment changes the ramp signal which is applied to the control circuit output voltage after the initial valve opening is achieved. Thus, as the pressure in the storage tanks decreases, the control valve opening increases to maintain the air flow over time at the initial setting. By manipulating these two adjustments, the wind tunnel may be operated at a reasonably constant air flow for a period of time. The duration of the steady flow is determined by the initial pressure in the storage tanks and the magnitude of the steady flow rate. The minimum run duration for this research was nominally 18 seconds.

Flow Straightener

The flow straightener which is located 1.041 m upstream of the test section inlet is employed to provide flow to the inlet of the test section with the highest degree of uniformity possible. A vertical traverse at the centerline of the test section inlet revealed virtually no nonuniformity in the total pressure of the inlet flow.

Test Section

The test section used during this research is shown in Figure 6. The inlet is rectangular, 15.24 cm wide and 37.26 cm high. Note that a transition piece just upstream of the test section inlet provides a smooth flow path as the wind tunnel cross-section changes from circular to rectangular. A moveable total pressure probe is located at the centerline of the test section, penetrating the roof of the test section, just downstream of the blade row. It is indexed in 2.54 cm increments, and is used to measure the uniformity of the flow at the blade row inlet, as discussed in the previous section. This total pressure probe is fully retracted

during operation of the wind tunnel when data is being recorded so as not to disturb the inlet flow.

The blade row consists of eleven turbine blades with identical geometry (Figure 7). The throat of the blade passages almost coincide with the blade trailing edge, and the blade row inlet Mach number is 0.2 when the flow is choked. The blades are mounted between two pieces of clear plexiglass to facilitate flow visualization, and the entire assembly (referred to as the *cascade*) may be removed from the test section as a unit (Figure 8). For convenient reference, the blades are numbered from one to eleven, and the blade passages are lettered A through J (Figure 9). As mentioned previously, the blades have identical geometry; however, the cascade consists of three groups of blades. Six of the blades (numbers 1, 2, 3, 9, 10 and 11) have no modification made to them. Two blades (numbers 7 and 8) have static pressure taps (0.254 mm D) drilled in them along the centerline of the blades in the flow direction (Figure 10). Blade number 7 has nine static taps drilled into its suction surface, and blade number 8 has five static taps drilled into its pressure surface and one into its trailing edge. Short lengths of stainless steel tubing (1.067 mm OD/ 0.635 mm ID) are connected to the static taps, and are routed inside the blades and through the cascade walls to allow connection of the taps to a pressure measuring system (Figure 11). The third group of blades (numbers 4, 5 and 6) are configured to allow fluid to be injected into the main flow from the trailing edges[1] (Figure 12). The blades are completely hollow, and have 0.794 cm holes in each end. Corresponding holes are drilled in the plexiglas walls of the cascade. Special fittings are inserted into these holes to allow connection to the coolant injection system (Figure 13). The coolant is exhausted through 40, 2.381 mm by 0.635 mm holes in the trailing edge of each cooled blade (Figure 14). The cooled blades do not have any static taps to measure the surface static pressure distribution.

---

[1] Heat transfer studies are not a part of this research; however, for the sake of brevity, the blades which are configured for trailing edge injection are referred to as *cooled blades* and the fluid which is delivered to the cooled blades is referred to as *coolant*.

The right-hand (facing in the flow direction) wall of the cascade has two groups of static pressure taps drilled into it at different horizontal distances from the trailing edge of the blades (Figure 15). Short (1.905 cm) pieces of 1.59 mm OD/0.79 mm ID stainless steel tubing are inserted and epoxied into the holes so that the static taps maybe connected to pressure transducers via flexible plastic tubing. The first set is located at $x = 4.76$ mm horizontally behind the trailing edges of the blades, which is referred to as the *forward* position. It consists of eleven holes in a vertical row spaced at 3.73 mm intervals such that the middle hole is directly in line with the trailing edge of blade number 6 in the design exit flow direction. Thus, it is possible to measure the static pressure distribution for one entire blade spacing; in this case from the middle of passage E to the middle of passage F. The second set is located at $x = 76.20$ mm horizontally behind the trailing edge of the blades, which is referred to as the *rear* position. It consists of three holes in a vertical row spaced at 18.63 mm intervals such that the lower tap is in line with the trailing edge of blade number 6 and the upper tap is in line with the trailing edge of blade number 7, both in the design exit flow direction.

Enclosing the sides of the test section are two aluminum doors with slots milled into their inside surfaces. When the doors are secured in position the slots engage the walls of the cascade which is then held rigidly in place. The aluminum doors have 10.80 cm by 15.24 cm openings cut into them which expose several blade passages (letters D, E and F) to visual observation (Figure 16). Penetrating the left-hand door (facing in the flow direction) is a fixed total pressure probe (1.588 mm OD/0.794 mm ID) which is offset 3.81 cm horizontally from the inside surface of the door.

The back wall of the test section is situated at an angle such that it is parallel to the design exit flow direction. A movable, solid tailboard is attached to the test section back wall by an arrangement of six adjusting bolts (Figure 17). By manipulating the adjusting bolts, the angle of the tailboard may be set as desired. The angle of the tailboard effectively sets the exit Mach number when the blade row is choked by fixing the area ratio $\frac{A}{A^*}$ where A^* is the

total throat area of the cascade row (A more complete discussion of the arrangement of the tailboard and it's use is given in [2]).

A 10.16 cm by 15.24 cm access hole is located on the floor of the test section into which the total pressure probe support fixture is inserted (Figure 18). A total pressure probe is inserted through the guide tube before the fixture is secured in place. This probe traverses vertically behind the blade row during operation of the wind tunnel. Since the probe enters through the floor of the test section and the uppermost blade passage which is traversed is 52.07 cm above the test section floor, the probe stem is quite long. The purpose of the probe support fixture (Figure 19) is to provide a smooth path for the probe during its traverse and to minimize bending of the probe as it extends.

3.2.1.2 Coolant Supply System

The coolant supply system, which provides a uniform flow of carbon dioxide[2] (CO_2) to each of the three cooled blades at a constant flow rate, is shown schematically in Figure 20. CO_2 is transferred from the high pressure (10.34 Mpa, 1500 psi) tanks in which it is received to a large tank where it is stored at low pressure (275-350 kPa, 40-50 psi). Flow of CO_2 from the storage tank is controlled by a solenoid valve. The CO_2 is delivered to a distribution manifold by a 4.88 m length of 1.905 cm ID copper tubing. The flowrate to the distribution manifold is controlled by a pressure regulator. The flow passed by the regulator is determined by the control pressure which is applied to it. As the control pressure increases, the CO_2 flowrate increases proportionately. The magnitude of the CO_2 flowrate is measured by a float-type flowmeter which is located just upstream of the distribution manifold. CO_2 is uniformly distributed from the manifold to the three cooled blades via six 76.20 cm lengths of

---

[2] Carbon dioxide was chosen as the coolant because its use closely simulates the density ratio between the injected fluid and the main flow fluid which is present in an actual gas turbine.

flexible plastic tubing. CO_2 is supplied to each cooled blade by two tubes, one at each end of the blade.

3.2.1.3 Experimental Procedure

Two general categories of data were recorded during the research. The first category is pressure data of various sorts which were recorded through the use of pressure transducers. The pressure data was recorded both in digital form on computer disks and in analog form on stripcharts. The second category of data is visual data. Still photographs were taken to record the shock structure of the flow in the blade passages and at the blade row exit utilizing the shadowgraph technique.

Pressure Data

As was mentioned above, several types of pressure data were recorded. The pressures recorded are:

1. Total pressure upstream of the blade row, $p_{t,1}$

2. Difference in total pressure across the blade row, Δp_t

3. Blade suction surface static pressure (9 locations), $p_{b,s,1-9}$

4. Blade pressure surface static pressure (6 locations), $p_{b,p,1-6}$

5. Wall static pressure, forward position (11 locations), $p_{w,f,1-11}$

6. Wall static pressure, rear position (3 location), $p_{w,r,1-3}$

$P_{t,1}$ was measured using the fixed total pressure probe which penetrates the left-hand door of the test section and a pressure transducer. $P_{t,1}$ was assumed to be uniform at the test section inlet.

Δp_t was measured by applying $p_{t,1}$ and $p_{t,2}$ to the high and low pressure inputs, respectively, of a differential pressure transducer. $P_{t,2}$ was measured using a total pressure probe which enters the bottom of the test section via the support fixture (Ref. Section 3.2.1.1). The total pressure probe was driven by a traversing mechanism which consists of a stepper motor, a reduction gear and a rack and pinion arrangement (Figure 21). The rack and pinion converts the rotational motion of the stepper motor drive axle to a linear motion with which to traverse the total pressure probe. The probe velocity was $v_p = 0.47$ cm/s during the traverse. This velocity was found through trial and error to be fast enough to record data for two blade spacings while the wind tunnel flow was held reasonably constant, yet slow enough so as not to exceed the response time of the instrumentation which would result in distortion of the data. Typically, the traverse started in the middle of passage C below the lower cooled blade (number 4), and ended in the middle of passage E above the middle cooled blade (number 5). Thus, the spatial variation of P_t, referred to as a *wake*, over two blade spacings was determined. Two blade spacings were traversed in order to demonstrate that an adequate level of periodicity was present in the cascade flow.

The blade surface static pressures $p_{b,s,1-9}$ and $p_{b,p,1-6}$, and the cascade wall static pressures $p_{w,f,1-11}$ and $p_{w,f,1-3}$ were measured using a multichannel pressure transducer. $P_{w,f,1-11}$ were used to calculate an average static pressure at the blade exit, $p_{2,avg}$[3]. $P_{2,avg}$ is ratioed with $p_{t,1}$ in order to calculate the blade exit Mach number $M_{2,isen}$. The isen(tropic) subscript is used because ratioing $p_{2,avg}$ with $p_{t,1}$ to calculate exit Mach number assumes that the flow through the blades is isentropic, which is only approximately true. The blade surface static pressures were ratioed with $p_{t,1}$ to give the local Mach number distributions on the suction and pressure surfaces of the blades.

---

[3] In the absence of an alternative, the static pressure at the center of the cascade is assumed to be equal to the cascade wall static pressure.

The measured parameters discussed above were recorded both in analog form and digital form during each run. The output signals of the $p_{t,1}$ and Δp_t transducers were recorded by a strip chart recorder. This method gives the variation of $p_{t,1}$ with time directly. Since the travel velocity of the stripchart paper was known, the variation of Δp_t with position is given implicitly. The advantage of recording data with a strip chart recorder is that the data is instantly available for examination for each run. In addition, the output signals of the $p_{t,1}$ and Δp_t and transducers were recorded on computer disk by a personal computer based data acquisition system. The data acquisition system recorded values for $p_{t,1}$ and Δp_t approximately 700 times during the time required for the total pressure probe to traverse two blade spacings (7.45 cm, approximately 16 sec). In contrast to the strip chart recorder data, this data gives the variation of Δp_t with vertical position directly. While this data requires processing to before it is available for analysis, the faster response time and higher resolution of the data make it more useful for accurate analysis than the strip chart data.

The data discussed in the previous section was recorded essentially continuously while the wind tunnel was operating. In contrast, $p_{b,s,1-9}$, $p_{b,p,1-6}$, $p_{w,f,1-11}$ and $p_{w,r,1-3}$ were recorded at one instant during operation of the wind tunnel, when $p_{t,1}$ reached its steady value. $P_{t,1}$ was also recorded at that instant. These data were recorded by a separate data recording system which is controlled by the same personal computer as the data acquisition system. This separate system is composed of one, 32-channel pressure transducer and a control unit which scans each channel in rapid succession. As each channel is scanned the pressure is read into memory. When all channels have been scanned the data is downloaded to the personal computer and stored on disk.

Visual Data

The second type of data recorded during the research is photographic images of the flow through the cascade. Flow visualization is an important tool for gaining an understanding of the fluid mechanics of any problem involving compressible flow. To this end, high speed

photographs were taken during those runs when local Mach numbers in the cascade flow were to be greater than one.

In order to obtain these photographs, the shadowgraph technique was employed. The shadowgraph system employed during the research consists of a high speed light source, a partially focussing lens, two concave mirrors, a plane mirror and a camera (Figure 22). The light source produces a 2.4 millisec spark of light which is directed through the lens and onto the first convex mirror. The focal lengths of the lens and the mirror are such that the light reflecting off of the mirror is a beam of parallel, or collimated, light. This light is directed through the windows in the test section doors, parallel to the trailing edges of the blades. After the light passes through the test section it is reflected off of the second concave mirror which focusses the light (and the image of the visible cascade blades and passages). The image is then reflected off of a plane mirror which directs the image into the camera to expose the film. In order to take a picture of the flow, the wind tunnel laboratory lights are turned off and the film is uncovered. The wind tunnel valve is then opened, and after the flow reaches its steady condition the spark is triggered which exposes the film. The underlying principle of the shadowgraph method is that the index of refraction of the medium flowing in the cascade is proportional to the density of the fluid. A higher density medium will refract light to a higher degree than a lower density medium. Since the light entering the test section is made up of parallel beams, regions containing large density gradients, i.e. shock waves, will refract light more and will show up on the film as shadows. Figure 23 is an example of a typical photograph obtained using this technique.

Photographs of the flow were taken using the shadowgraph technique under many flow conditions in an attempt to discern what, if any, effect the trailing edge injection had on the shock structure. These photographs captured the shock structure in the flow, especially at the trailing edge. Of particular interest was the shock/boundary layer interaction involving an oblique shock from the trailing edge of one blade intersecting with the boundary layer growing on the suction side of an adjacent blade (Figure 23). The influence of an oblique

shock impinging on a surface on which a boundary layer is growing causes the boundary layer to separate and then quickly reattach. Oblique shocks are formed as the flow is turned both when the flow separates and when it reattaches. Thus the impinging shock appears to cause a *double* reflection. Further discussion of this effect is given by Shapiro [15]. Also of interest was the strength of reflections of oblique shocks from the trailing edges of blades off of the solid tailboard (Figure 23). These reflected shocks are unwanted disturbances in the cascade flow, and attempts were made to minimize their strength. Reference [2] gives further discussion on reflected shocks and the methods employed to minimize their effect.

An alternative to the shadowgraph method is the Schlieren method. This method is much more sensitive to density gradients than is the shadowgraph method; however, due to the obscuring effect of oil vapor present in the wind tunnel air which collected on the cascade walls, this method was not used. For a more complete discussion of the shadowgraph and Schlieren methods of flow visualization, see [16].

3.2.2 Testing Program

In order to examine the effect that trailing edge injection has on the aerodynamic performance of gas turbine blades, the procedures described in Section 3.2.1.3 were conducted under a number of different test conditions. The parameters which were varied are the blowing rate, B, the isentropic blade row exit Mach number, $M_{2,isen}$, and the horizontal distance behind the blade trailing edge at which Δp_t was measured.

First data was taken with no injection at all in order to establish the baseline performance of the blades. Data was then recorded for two values of B: i.e., B = 0.27 and B = 0.54. Another variable test condition was the blade row exit Mach number, $M_{2,isen}$. Tests were conducted at values of $M_{2,isen}$ ranging from 0.79 to 1.36. In order to determine what effect

trailing edge injection might have on development of the wakes behind the blades, measurements were taken at three positions downstream of the blade trailing edge in the flow direction. The measurement positions were located at $\frac{x}{c} = 1.125$, $\frac{x}{c} = 1.667$ and $\frac{x}{c} = 3$; where $\frac{x}{c} = 0$ and $\frac{x}{c} = 1$ are the leading and trailing edges, respectively, of the blades (Figure 24).

Thus, for each value of $M_{2,iso}$ tested, data was recorded for three values of B at three horizontal distances from the blade trailing edge. Figure 25, Figure 26 and Figure 27 show examples of wakes taken at each measurement location. Table 1 through Table 3 delineates all of the combinations of test conditions under which data was recorded.

3.3 Description of Results

Section 3.2 discussed in detail the equipment used to collect the experimental data, and the various test conditions under which the data was obtained. This section will provide the results of the testing program, the methods and assumptions used in reducing the raw data and an analysis of these results. An estimate of the accuracy of the data will be presented in order to establish the validity of any conclusions which are made as a result of this research.

3.3.1 Reduction of Data

As was discussed previously, data was collected under a variety of testing conditions as delineated in Table 1 through Table 3. The data collected for each test case consists of the following:

1. $P_{t,1}$ and Δp_t recorded at 700 points over two blade passages (7.45 cm).

2. $P_{t,1}$, $p_{bl,s,1-9}$, $p_{bl,p,1-8}$, $p_{w,f,1-11}$, and $p_{w,r,1-3}$ recorded simultaneously at one instant during each run.

The raw data was reduced using a computer program which calculated $\bar{L}$ for each test case. These results will be presented in both tabular and graphical format to establish the effect of trailing edge injection on the performance (as quantified by $\bar{L}$) of the gas turbine blade.

3.3.1.1 Raw Data Reduction Algorithm

This section describes each step of the algorithm that the computer program follows in reducing the raw data.

Convert Raw Data

Before the data could be manipulated, it had to be coverted into a useable form. $P_{t,1}$ and Δp_t were recorded digitally, that is the output voltages of the transducers were converted proportionately by the computer based data acquisition system into numbers and stored. The constant of proportionality depends upon the input voltage range of the data acquisition system. After the digital data was converted back into volts, the voltages were converted into gage pressures via known transducer calibrations. Finally, the pressures were converted to absolute pressures using the local atmospheric pressure which was recorded each testing day. The data collected once each run were recorded directly as gage pressures so they only had to be converted to absolute pressures.

Calculate P_2 and $P_{t,2,prb}$

When the blade row exit Mach number was greater than one, a bow shock formed in front of the tip of the total pressure probe. The total pressure loss across the bow shock had to be allowed for in order to calculate the true total pressure. Details of the correction will be presented in the next section. The correction method is different depending upon whether or not the tailboard was installed. The following discussion pertains to the case where the tailboard was installed.

Two parameters which had to be determined in order to correct for the probe bow shock are the static pressure downstream of the blade row, p_2, and the total pressure measured by the total pressure probe, $p_{t,2,prb}$. At any horizontal measurement location, p_2 was assumed to be the average of the wall static pressures at that location and thus was known at the forward and rear measurement locations at one instant for each run. The static pressure was assumed to vary linearly between the forward and rear measurement locations so that the static pressure at the middle measurement location at one instant could also be determined. One input to the data reducing computer program is the horizontal measurement location at which the total pressure probe traversed behind the blade row for each data set. Based on this input the appropriate value was assigned to p_2. Recall that p_2 was only measured once during a run. In order to determine p_2 at each point in the traverse it was assumed that, with the tailboard installed, the exit Mach number (and $\frac{p_{t,1}}{p_2}$) remained constant. $P_{t,1}$ was recorded simultaneously with the wall static pressures so that one value of $\frac{p_{t,1}}{p_2}$ (assumed constant) was known. Since $p_{t,1}$ was also recorded at each point in the traverse, p_2 could be determined at each point in the traverse.

Δp_t was also recorded at each point in the traverse so that $p_{t,2,prb}$ was determined simply by subtracting Δp_t from $p_{t,1}$.

Calculate $P_{t,2}$ and P_t

As stated above, the presence of supersonic flow at the blade row exit implies the existence of a bow shock in front of the total pressure probe which had to be accounted for to determine $p_{t,2}$. Of course, for subsonic exit flow, $p_{t,2} = p_{t,2,prb}$. M_2 was then determined via the isentropic relationship

$$\frac{p_{t,2}}{p_2} = \left[1 + \frac{(\gamma - 1)}{2} M_2^2\right]^{\frac{\gamma}{(\gamma - 1)}} \quad [3.5]$$

However, for supersonic exit flow, the total pressure measured by the probe was less than the actual total pressure due to the total pressure loss across the bow shock. This would result in an exaggeration of the total pressure loss across the blade row. In some cases, the blade row exit flow was supersonic in certain regions (i.e., the middle of the blade passage) and subsonic in other regions (i.e., the wake region behind the blade trailing edge). In order to test for a supersonic flow condition, $p_{t,2,prb}$ was ratioed with p_2. If this ratio was greater than 0.528, a probe bow shock was present.

For the purpose of calculation, the probe bow shock is treated as a normal shock. M_x and $p_{t,x}$ are the Mach number and total pressure upstream of the normal shock, and M_y and $p_{t,y}$ are the Mach number and total pressure downstream of the normal shock. $P_{t,y}$ is equivalent to $p_{t,2,prb}$. $P_{t,x}$ and p_2 are related by the isentropic relation

$$\frac{p_{t,x}}{p_2} = \left[1 + \frac{(\gamma - 1)}{2} M_x^2\right]^{\frac{\gamma}{(\gamma - 1)}} \quad [3.6]$$

$P_{t,x}$ and $p_{t,y}$ are related by the normal shock relation

$$\frac{p_{t,x}}{p_{t,y}} = \left[\frac{\frac{(\gamma + 1)}{2} M_x^2}{1 + \frac{(\gamma - 1)}{2} M_x^2}\right]^{\frac{\gamma}{(\gamma - 1)}} \left[\frac{1}{\frac{2\gamma}{\gamma + 1} M_x^2 - \frac{\gamma - 1}{\gamma + 1}}\right]^{\frac{1}{\gamma - 1}} \quad [3.7]$$

Once $p_{t,y}$ and p_2 were known, Eqns. 3.6 and 3.7 were solved simultaneously to calculate M_x at each point in the traverse. Note that $M_x = M_2$. After M_x was determined, $p_{t,x}$ was calculated via Eqn 3.6.

The discussion above is relevant to testing when the tailboard is installed. Without the tailboard installed, the assumption that $\frac{p_{t,1}}{p_2}$ is constant is no longer valid. In this case, M_2 was calculated using an empirically determined relationship between $p_{t,1}$ and $M_{2,isen}$. An assumption was made that $M_2 = M_{2,isen}$. $P_{t,x}$ was then calculated via Eqn. 3.7.

After $p_{t,x}$ was determined, P_t (Eqn. 3.2) could be calculated at each point in the traverse such that $p_{t,2} = p_{t,x}$ when the exit flow was supersonic and $p_{t,2} = p_{t,2,prb}$ when the exit flow was subsonic. Figure 28 shows the effect that the probe bow shock correction has on the calculation of P_t and $\bar{L}$. Naturally, the effect of the bow shock is most significant at higher values of $M_{2,isen}$, and approaches zero as $M_{2,isen} \to 1$. For example, at $M_{2,isen} = 1.36$ $\bar{L}$ is 38 percent lower when the data is corrected for a bow shock. In contrast, $\bar{L}$ is reduced by only 3.5 percent for $M_{2,isen} = 1.08$

Calculate ρ_2 and V_2

After P_t was calculated, the only parameters that had to be determined in order to calculate $\bar{L}$ were ρ_2 and V_2. In order to calculate these parameters, the static temperature T_2 first had to be determined from the isentropic relation

$$\frac{T_{t,2}}{T_2} = \left[1 + \frac{(\gamma - 1)}{2} M_x^2 \right] \quad [3.8]$$

Since there were no means available to measure the downstream total temperature $T_{t,2}$, it was assumed to be equal to $T_{t,1}$. As was discussed above, M_2 was determined at each point in the traverse; therefore, T_2 could be determined at each point in the traverse via Eqn. 3.8. After

calculating T_2, ρ_2 was calculated via the ideal gas law and V_2 was calculated via the definition of Mach number. Thus

$$p_2 = \rho_2 R T_2 \quad [3.9]$$

$$V_2 = M_2 \sqrt{\gamma R T_2} \quad [3.10]$$

Calculate $\bar{L}$

Having determined the required parameters, $\bar{L}$ was calculated via Eqn. 3.3. The integration was carried out using the trapezoidal rule method for numerical integration. The trapezoidal rule for the integration of an arbitrary function $f = f(y)$ is

$$\int_a^b f(y)\, dy = \frac{\delta y}{2}\left[f(a) + f(b)\right] + \sum_{i=2}^{n-1} \delta y\, f_i(y) \quad \text{where } n = \frac{(a-b)}{\delta y} \quad [3.11]$$

δy is the change in position of the probe between measurement points and is a calculated quantity. The position of the probe was measured using a linear velocity/displacement transducer (LVDT); however, due to unavoidable electrical noise in the instrumentation system which produced significant scatter in the LVDT output, the calculated value of δy is considered to yield more accurate values of $\bar{L}$.

It is noted that the velocity u in Eqn. 3.3 is the velocity normal to the direction of integration. For lack of better information, the blade row exit flow direction was assumed to be parallel to the blade exit angle β_2. Therefore, $u = V_2 \cos(68°)$

3.3.1.2 List of Assumptions

A number of assumptions were made when developing the data reduction algorithm discussed above. The following list delineates all assumptions which were made so as to preclude any ambiguity when interpreting the results. Where any assumption is considered to have a significant influence on the accuracy of the results, this will be noted and discussed in the uncertainty analysis (Section 3.4). The assumptions which were made are:

1. The static pressure downstream of the the blade row was assumed to be equal to the static pressure measured by the cascade wall static taps. This assumption neglects any pressure gradient between the cascade wall and the centerline of the cascade. This assumption was necessary because there were no means available to measure the static pressure at the cascade centerline.

2. The static pressure was assumed to vary linearly between the forward and rear measurement locations. This assumption neglects the effect of any shocks which may be present between the two locations.

3. The ratio $\frac{p_{t,1}}{p_2}$ is assumed to remain constant for the duration of a run when the tailboard is installed. This assumption is based on the fact that $M_{2,isen}$ (and $\frac{p_{t,1}}{p_2}$) is determined by the value of $\frac{A}{A^*}$ which results from a particular tailboard angle. Thus, in theory, $M_{2,isen}$ will remain constant as long as the tailboard angle is not changed. In practice, however, the tailboard vibrates and deflects under dynamic loads while the wind tunnel is operating. Therefore, $\frac{p_{t,1}}{p_2}$ will vary to a small degree over the duration of a run.

4. When the tailboard is not installed, M_2 was assumed to be equal to $M_{2,isen}$. This assumption was made due to the lack of means to measure p_2 at the cascade centerline. Thus, M_2 could not be calculated via Eqns. 3.6 and 3.7. Therefore, a relationship between

$M_{2,isen}$ and $p_{t,1}$ was derived experimentally. This allowed M_2 to be calculated at each point in the traverse when the tailboard was not installed.

5. $T_{t,2}$ was assumed to be constant and equal to $T_{t,1}$. This assumption was made due to a lack of means to measure $T_{t,2}$. As an estimate, $T_{t,1}$ was measured upstream of the test section using a thermocouple under what were considered *typical* flow conditions. In the pipe upstream of the test section, the Mach number is quite low (approximately 0.13) for choked flow so a recovery factor of 1 was used when measuring $T_{t,1}$ with a thermocouple. Since $T_{t,1}$ varies somewhat over the duration of a run due to the pressure drop in the wind tunnel storage tanks, $T_{t,2}$ was equated the average of the measured values of $T_{t,1}$ for a run under typical conditions. It is noted that the effect of having a somewhat rough estimate $T_{t,2}$ only affects the calculated value of B. The effect on $\bar{L}$ is negligible because the parameters which are calculated using $T_{t,2}$ (i.e., ρ_2 and V_2) appear in both the numerator and denominator of Eqn. 3.3.

6. The fluid flowing through the cascade was assumed to be an ideal gas with $\gamma = 1.4$ and $R = 0.287 \frac{kJ}{kg\ K}$. This assumption neglects the mixing of a small amount of CO_2 into the main flow of air.

7. The exit flow was assumed to be at the design angle of 68°. This is not strictly true due to the shock structure at the trailing edge of the blades. An implied assumption is that the probe is aligned with the flow direction. This assumption is also not strictly true since the probe is subject to deflection under dynamic loads while the wind tunnel is running. This source of error is is not considered significant as it is generally accepted that the error in pressure measurement due to probe misalignment is proportional to $(1 - \cos \alpha)$, where α is the angle between the flow direction and the probe direction. For example, the error due to a 5° misalignment is approximately 0.4 percent.

3.3.2 Results

The results of the research are given in both tabular and graphical formats. The tabulated results are shown in Table 1 through Table 3. The information consists of the measurement location ($\frac{x}{c}$), the blowing rate B and the isentropic Mach number $M_{2,isen}$ for each data set. Also included is the average isentropic Mach number $M_{2,isen,avg}$ as a means of grouping all the data sets taken with the same tailboard angle when the data was taken with the tailboard installed. The reason that $M_{2,isen}$ does not remain precisely constant within groups of data taken with the same tailboard position is given in the previous section.

The graphical results are given in a series of plots shown in Figure 29 through Figure 37. Figure 29 through Figure 31 are families of curves showing $\overline{L}$ vs. $M_{2,isen,avg}$ for each measurement location. Each curve within a family represents a different value of B. Figure 32 through Figure 37 are families of curves showing $\overline{L}$ vs. measurement location for each $M_{2,isen,avg}$. Again, each curve within a family represents a different value of B. Both types of plot show the effect of B on $\overline{L}$. The first group of plots also shows the effect of $M_{2,isen,avg}$ on $\overline{L}$, and the second group of plots also shows the effect of distance behind the blade trailing edge on $\overline{L}$.

Figure 38 through Figure 42 provide samples of the blade pressure distributions and shadowgraphs for information. The full data sets are not provided as it was found that B had no discernable effect on either the pressure distributions or the shock structure for a given $M_{2,isen,avg}$. Figure 38 through Figure 42 are provided to illustrate the effect of $M_{2,isen,avg}$ on the pressure distributions and the shock structure.

Figure 38, Figure 39 and Figure 40 show the blade surface pressure distributions for $M_{2,isen,avg} = 0.79$, 1.08 and 1.36 . Each figure shows the pressure distributions for B=0, B=0.27

and B = 0.54. Figure 41 and Figure 42 show shadowgraphs taken for $M_{2,isen,avg}$ = 1.08 and 1.36. Each figure shows the shock structure for B = 0 and B = 0.54.

3.3.3 Analysis

Comparison of Figure 29, Figure 30 and Figure 31; and Figure 32 through of Figure 37 reveals few clear trends of the effect of B on $\bar{L}$. The high subsonic case ($M_{2,isen,avg}$ = 0.79) shown in Figure 32 is the only group of data which shows a clear relationship between B and $\bar{L}$. In this case, B = 0.27 yields a higher $\bar{L}$ than does B = 0, and B = 0.54 yields a lower $\bar{L}$ than does B = 0. For all other values of $M_{2,isen,avg}$ (Figure 33 through Figure 37), the data does not clearly suggest any such relationship between B and $\bar{L}$. The data does suggest that, whatever the relationship between B and $\bar{L}$ may be, it is of such low magnitude that it is lost within the uncertainty of the data which is estimated at ± 12 percent (see Section 3.4- Uncertainty Analysis). This could account for the seemingly random relationship between B and $\bar{L}$ which is suggested by these data. Thus the data indicates that trailing edge injection has little effect on the performance of the turbine blade.

What is more clearly indicated by the data is the effect of $M_{2,isen,avg}$ on $\bar{L}$. Figure 29 through Figure 31 suggest a quadratic relationship between $M_{2,isen,avg}$ and $\bar{L}$.

Another phenomenon of interest is indicated by Figure 32 through Figure 37. These plots show that, for $M_{2,isen,avg}$ = 0.79, 1.08, 1.14 and 1.21 , $\bar{L}$ increases rapidly between $\frac{x}{c}$ = 1.125 and $\frac{x}{c}$ = 1.667 , and then remains essentially constant through $\frac{x}{c}$ = 3. For $M_{2,isen,avg}$ = 1.29, $\bar{L}$ continues to increase through $\frac{x}{c}$ = 3 , but not as rapidly. For $M_{2,isen,avg}$ = 1.36 $\bar{L}$ increases at nominally the same rate from $\frac{x}{c}$ = 1.125 through $\frac{x}{c}$ = 3. This suggests that, for lower exit Mach numbers, the loss is developed within one chord length of the trailing edge. As the exit Mach number increases, this interval increases. At the highest

exit Mach number tested ($M_{2,isen,avg} = 1.36$), the loss does not appear to be fully developed through two chord lengths downstream of the blade trailing edge.

3.4 Uncertainty Analysis

This section is included in order to provide an estimate of the accuracy of the data. Inaccuracies in the data may may occur for a variety of reasons. At the most basic level, the raw data will be somewhat in error due to inaccuracies in the instrumentation. The reduced data will have a degree of error introduced by the assumptions made in reducing the the data. Errors in the basic data elements will be estimated. Finally an estimate of the uncertainty in the results will be given.

The uncertainty, U, in $\overline{L}$ is expected to be no larger than the largest error in the values of P_t calculated at each point in the traverse. The errors in the calculated values of ρ, u, and δy are considered to have a small influence on $U_{\overline{L}}$ because these parameters appear in both the numerator and the denominator of Eqn. 3.3. The method suggested by Abernethy, et al. [17] is used as a guide in estimating $U_{\overline{L}}$.

Using the nomenclature of Abernethy, et al., uncertainty U is composed of the precision factor S, and the bias factor b, via

$$U = (b + t_{95}S) \quad [3.12]$$

The factor t_{95} is a statistical parameter that, for the purpose of this analysis will be a constant equal to 2.0. S is a measure of the repeatability of data and represents random error. The bias b represents inaccuracies in data due to systematic errors.

Since P_t is calculated from the measured quantities $p_{t,1}$ and Δp_t, $U_{P_{t,1}}$ will be composed of the uncertainties of these parameters. $P_{t,1}$ is assumed to be uniform; however, a traverse upstream of the cascade at mid-span shows that $p_{t,1}$ varies up to approximately 0.5 percent. In addition, analysis of the $p_{t,1}$ transducer calibration shows a maximum error of 0.25 percent. This error is the largest difference between the calibration data points and the least squares fit through these points. These components are combined following following Abernethy, et al. to give $b_{P_{t,1}} = 0.56$ percent. Analysis of the Δp_t transducer calibration yields an estimate for $b_{\Delta p_t}$ of approximately 0.5 percent. The repeatability of $p_{t,1}$ and Δp_t were not rigorously tested, so values for S are not available. However, experience dictates that $U_{P_{t,1}}$ is approximately 10 percent and $U_{\Delta p_t}$ is approximately 5 percent. Thus it may be seen that b is negligible compared to S for $p_{t,1}$ and Δp_t

Two methods were used to calculate P_t depending on the cascade exit flow conditions. If $M_2 \leq 1$, then P_t is calculated via Eqn. 3.2. Following Abernethy, $U_{P_{t,1}}$ and $U_{\Delta p_t}$ are combined to give an uncertainty for P_t of 12 percent.

P_t is calculated using more complex relationships when $M_2 > 1$ due to the correction for the probe tip bow shock. This would make the calculation of $U_{\Delta p_t}$ considerably more difficult to calculate directly using the method of Abernethy, et al.. The main difficulty stems from the fact that M_2 must be solved for iteratively. In any event, since the bow shock correction is relatively small, it is considered that the uncertainty due to the correction is correspondingly small and may be neglected. Thus, the uncertainty in $\bar{L}$ is given as

$$U_{\bar{L}} = \pm 12 \text{percent}$$

It should be noted that the preceding discussion is provided in order to estimate the maximum error which may be present in the results, and as such is considered to be conservative.

4.0 Conclusions and Recommendations

The goal of the research documented by this thesis was to determine the effect of trailing edge injection on the aerodynamic performance of a gas turbine blade. A number of conclusions and recommendations may be made based on the data collected during this research.

4.1 Conclusions

The most important conclusion is that, for the blades tested, trailing edge injection appears to have little effect on the loss coefficient of the turbine blade for values of $M_{2,isen}$ in the range from approximately 0.8 to 1.35. This would indicate that, with the turbine blade exit Mach number in this range, cooling of gas turbine blades via trailing edge injection may be expected to have little influence on the turbine efficiency from an aerodynamics point of view. In the case of B = 1, this result would not be wholly unexpected. From the definition of B it can be seen that for B larger than 1 the injected fluid would add momentum to the main flow. As a result, for $B \geq 1$ it was expected that no additional loss would be incurred. Indeed a small

reduction in $\overline{L}$ would be anticipated for values of B greater than one. It was thought that an increase in $\overline{L}$ might occur in the range $0 \leq B \leq 1$. No clear relationship between B and $\overline{L}$ was found, though B did have some effect on $\overline{L}$. However, this effect was noted to be small in most cases.

More conclusive relationships were noted between $M_{2,isen,avg}$ and $\overline{L}$, and between distance behind the blade trailing edge and $\overline{L}$. The relationship between $M_{2,isen,avg}$ and $\overline{L}$ was found to be approximately quadratic as suggested by Ainley and Mathieson [12]. With respect distance from the blade trailing edge, $\overline{L}$ was found to reach nearly its fully mixed value within one axial chord length from the blade trailing edge for exit Mach numbers up to approximately 1.2. As the exit Mach number increases, the point at which $\overline{L}$ reaches its fully mixed value was found to be further downstream of the blade trailing edge. For $M_{2,isen,avg} = 1.36$, $\overline{L}$ was found to not have reached its fully mixed value within two axial chord lengths of the blade trailing edge. In this case, however, shocks or reflections may have been present downstream of the cascade trailing edge which were not accounted for, but would contribute to total pressure losses.

As noted in Chapter 2.0, the results found in the literature relative to the effect of trailing edge injection are not unanimous. It is noted that results of the present research relative to P_t vs. $M_{2,isen}$ are similar to those given by Kacker and Okapuu [11]. Also, the result regarding the development of $\overline{L}$ downstream of the cascade correlates well with the result of Xu and Denton [9].

4.2 Recommendations

As a result of the research, the author considers the following recommendations to be appropriate:

1. Having established that trailing edge injection has no significant effect on the aerodynamic efficiency of the turbine blade, similar research should be carried out with a combination of trailing edge injection and film cooling.

2. Further research should be conducted to examine more closely how the loss develops far downstream of the blade trailing edges, especially at higher cascade exit Mach numbers. This might provide insight into the interaction between adjacent stages in a gas turbine.

3. The author considers that much of the scatter in the data is attributable to the integration of P_t. The calculated value of $\bar{L}$ was found to be influenced to a degree by the choice of where to start the numerical integration. When conducting similar research, it is recommended that considerable attention be paid to the interval over which data is recorded, and that a significant buffer of 'extra' data be recorded both before and after the intended region of integration.

4. Finally, it is recommended that the control system for the VPI&SU Cascade Wind Tunnel be replaced. The author considers that more accurate data could be obtained if the flow conditions were held more constant than is possible with the current electro-pneumatic system. The author considers that a feedback control system based on test section inlet flow conditions (i.e. total or static pressure) would be appropriate.

5.0 References

1. Van Wylen, G. J., and R. E. Sonntag, **Fundamentals of Classical Thermodynamics**, John Wiley & Sons, 1978, p.186.

2. Zaccaria, M. A., *Development of a Transonic Turbine Cascade Facility*, **M. S. Thesis**, Virginia Polytechnic Institute and State University,1988.

3. Kiock, R.,et al., *The Transonic Flow Through a Plane Turbine as Measured in Four European Wind Tunnels*, **ASME Paper No. 85-IGT-44**,1985.

4. Oates, G. C., *Chapter 12-Cascade Flows*, **The Aerothermodynamics of Gas Turbine Aircraft Engines**, Oates, G. C., Editor, Air Force Aero Propulsion Laboratory Report Number AFAPL TR-78-52,1978.

5. Gostelow, J. P., *The Present Role of High Speed Cascade Testing*, **ASME Paper No. 81-GT-95**,1981.

6. MacMartin, I. P., and J. F. Norbury, *The Aerodynamics of a Turbine Cascade With Supersonic Discharge and Trailing Edge Blowing*, **ASME Paper No. 81-GT-95**,1981.

7. Venidiktov, V. D., *Investigating a Turbine Stage With Cooling Air Leaving Through Slots in the Concave Surfaces of the Nozzle Blades*, **Teploenergetika**,1972.

8. Lawaczeck, O., *The Influence of Jets of Cooling Air Exhausted From the Trailing Edges of a Supercritical Turbine Cascade on the Aerodynamic Data*, **AGARD CP 229 Paper No. 30**,1977.

9. Xu, L. and J. D. Denton, *The Base Pressure and Loss of a Family of Four Turbine Blades*, **ASME Paper No. 87-GT-202**,1987.

10. Sieverding, C. H., *The Influence of Trailing Edge Ejection on the Base Pressure in Transonic Turbine Blades*, **ASME Paper No. 82-GT-50**,1982.

11. Kacker, S. C., and U. Okapuu, *A Mean Line Prediction Method for Axial Flow Turbine Efficiency* **ASME Paper No. 81-GT-58**,1981.

12. Ainley, D. G. and G. C. R. Mathieson, *A Method of Performance Estimation for Axial Flow Turbines* **N.G.T.E. Report r111, R&M No. 2974**,1951.

13. Dunham, J., and P. M. Came, *Improvements to the Ainley/Mathieson Method of Turbine Performance Prediction*, **ASME Journal of Engineering for Power**, July 1970, pp. 252-256.

14. Haller, B.R. and J-J Camus, *Aerodynamic Loss Penalty Produced by Film Cooling Transonic Turbine Blades*, **ASME Paper No. 83-GT-77 Power**, 1983.

15. Shapiro, A. H., **The Dynamics and Aerodynamics of Compressible Fluid Flow**, Robert E. Kreiger Publishing, 1987, pp. 1138-42.

16. Saad, M. A., **Compressible Fluid Flow**, Prentice-Hall, 1985, pp. 509-515.

17. Abernethy, R. B., et al., and J. W. Thompson, **Handbook, Uncertainty in Gas Turbine Measurements**, Arnold Engineering Development Center, United States Air Force, 1973, revised 1980.

Appendix A. Figures

INLET
FLOW

PRESSURE
SURFACE

SUCTION
SURFACE

EXIT FLOW
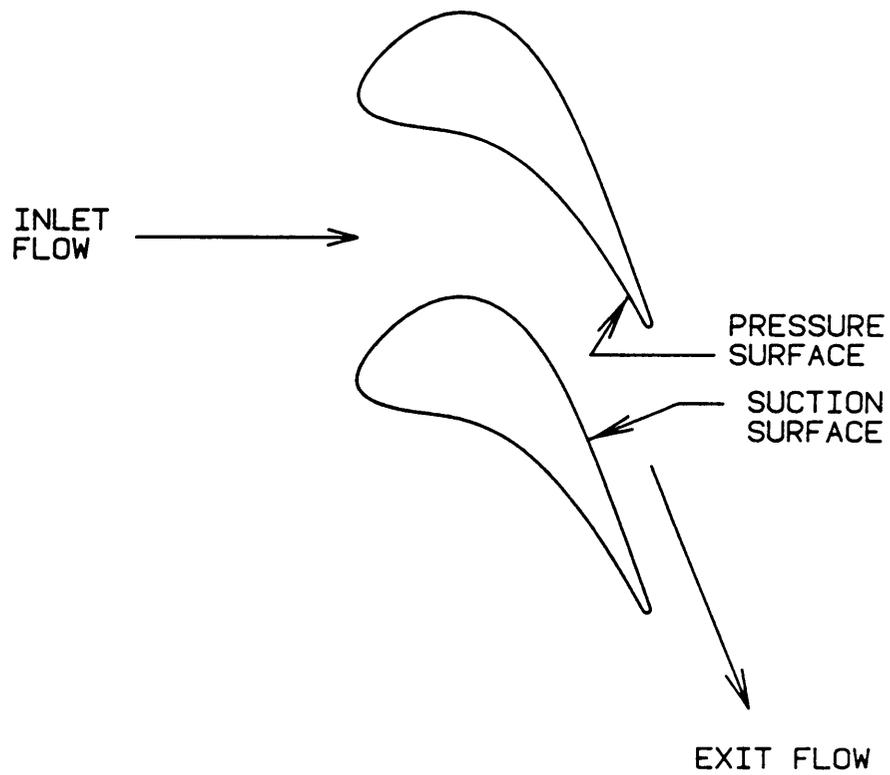
Figure 1.   Definition of a Blade Passage
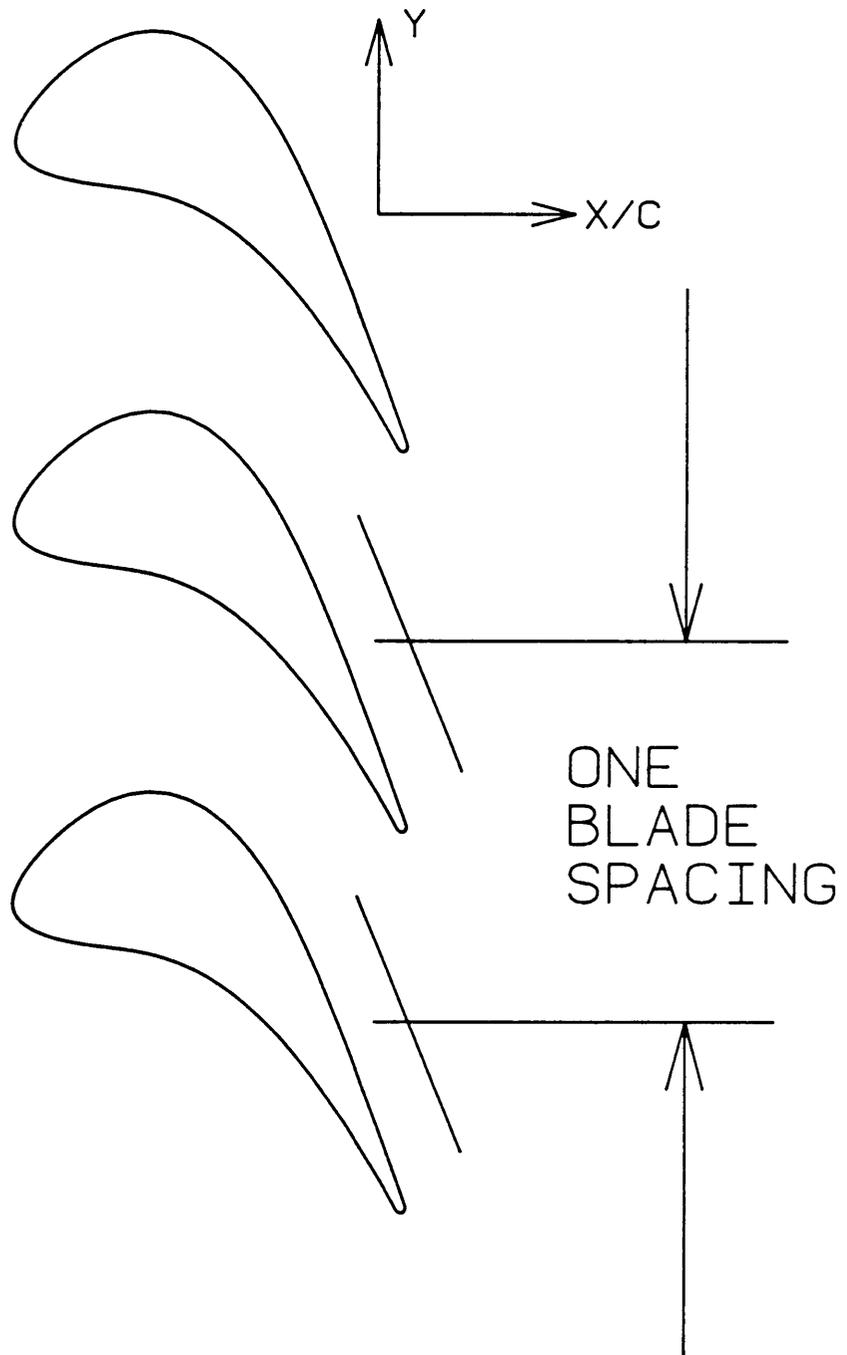
Figure 2. Region of Integration to Calculate Loss, With Coordinate System Shown
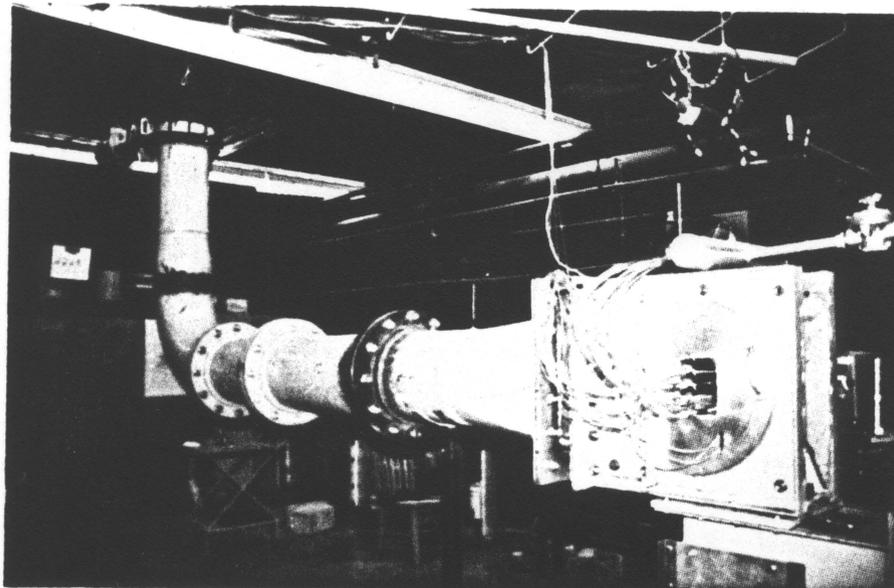
Figure 3. Wind Tunnel: A photograph of the VPI&SU Transonic Cascade Wind Tunnel. Note the test section at lower right.
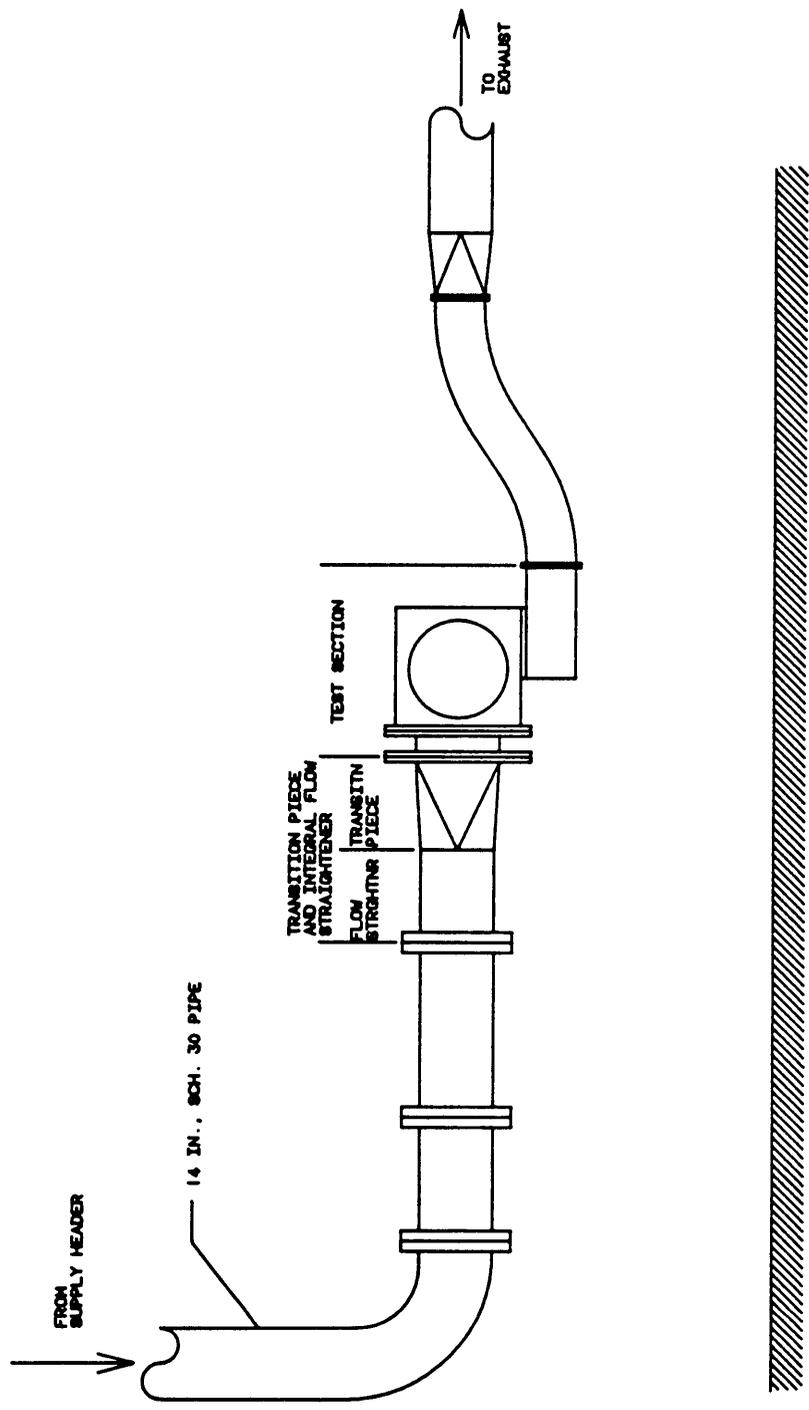
Figure 4. Wind Tunnel: A drawing of the VPI&SU Transonic Cascade Wind Tunnel with the major components identified.

STORAGE
TANKS

STORAGE TANK
PRESSURE TRANSDUCER

ACTUATOR
AIR
SUPPLY

WIND TUNNEL
SUPPLY HEADER

PNEUMATIC CONTROL
VALVE AND OPERATOR

TO TEST
SECTION

ELECTRO-PNEUMATIC
CONVERTER

VALVE CONTROL
CIRCUIT

REFERENCE
PRESSURE
SOURCE

ELECTRICAL
SIGNAL

PRESSURE
SIGNAL
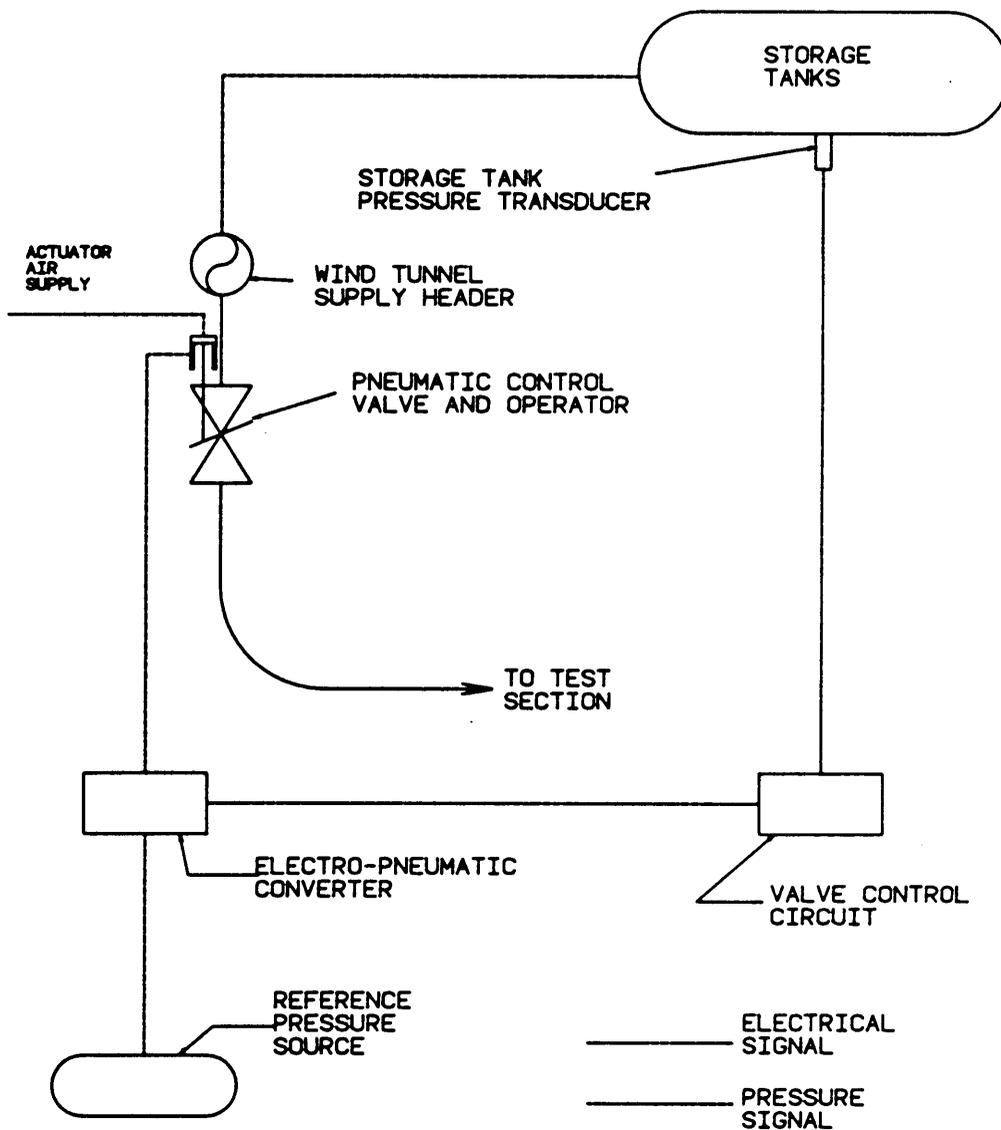
Figure 5. Control Valve Operating System Schematic
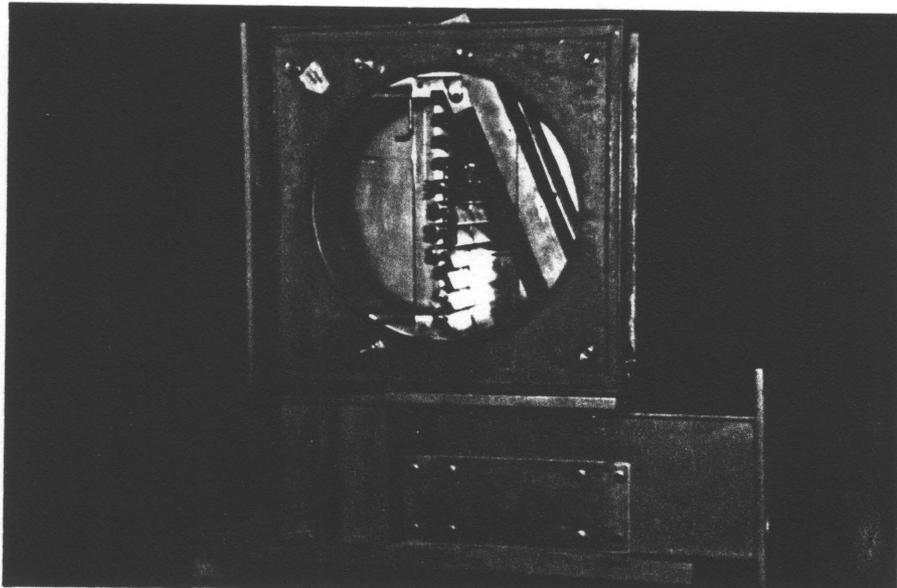
Figure 6. Test Section: A photograph of the test section.

CHORD=38.100 MM
SPACING=37.363 MM
INLET FLOW ANGLE=0 DEG
DESIGN EXIT FLOW ANGLE=-68 DEG
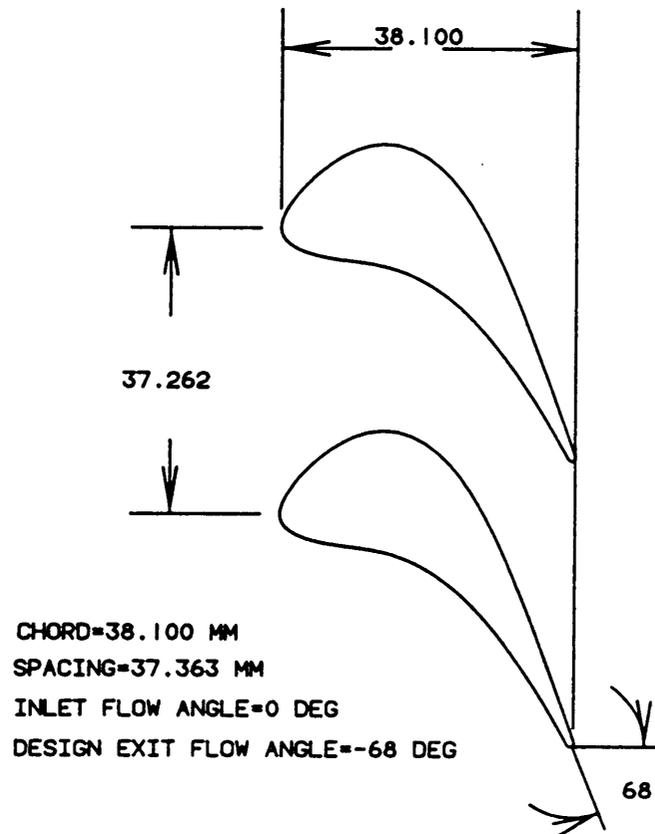
Figure 7.   Blade Geometry
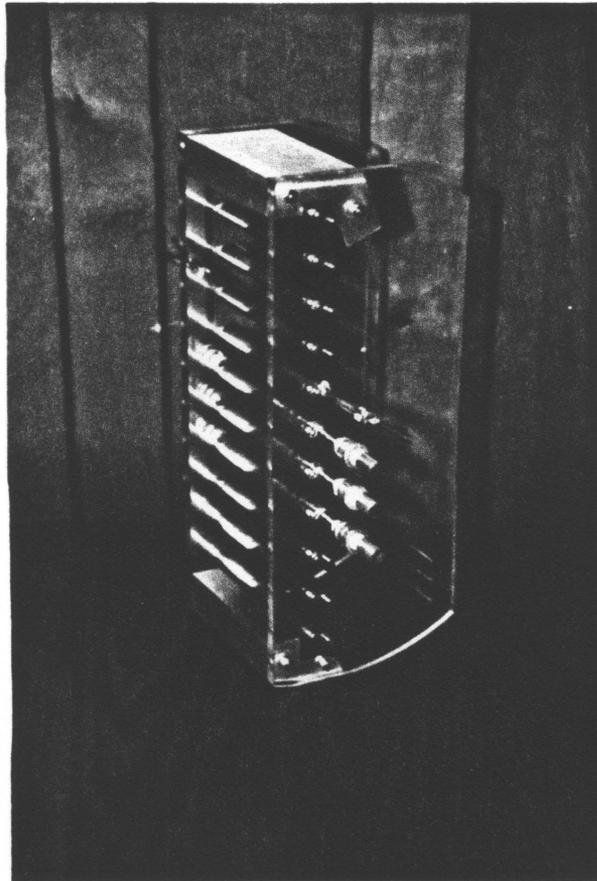
Figure 8. Cascade: A photograph of the cascade which was tested.
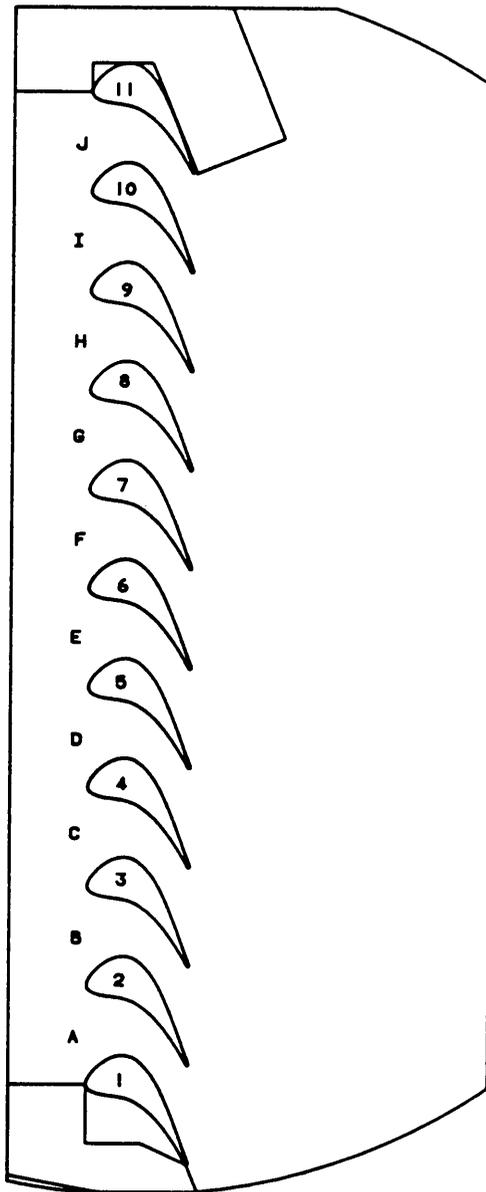
Figure 9. Definition of Reference Numbers for Blades and Reference Letters for Passages
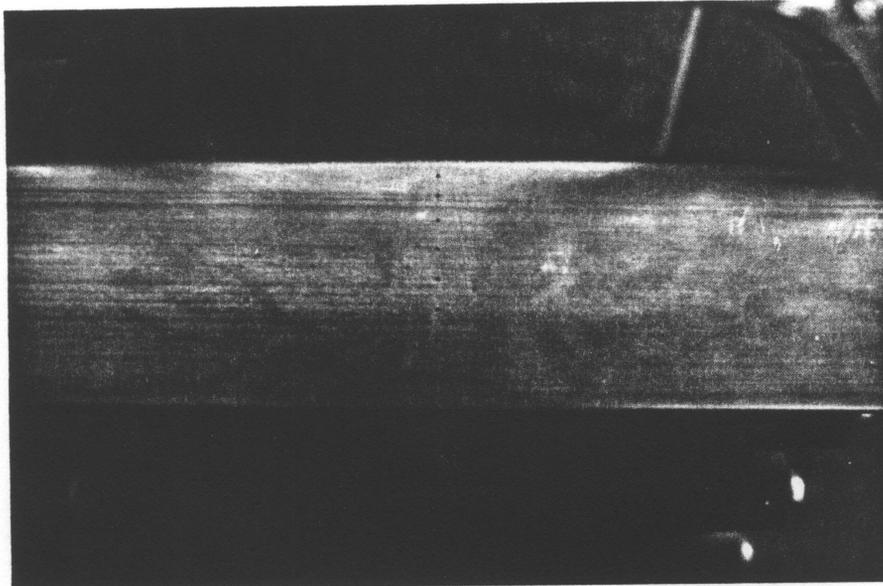
Figure 10.   Static Pressure Taps In Blade Surfaces: A photograph of the 0.254 mm D static taps drilled into the suction surface of blade 7. Similar holes are drilled into the pressure surface and trailing edge of blade 8.
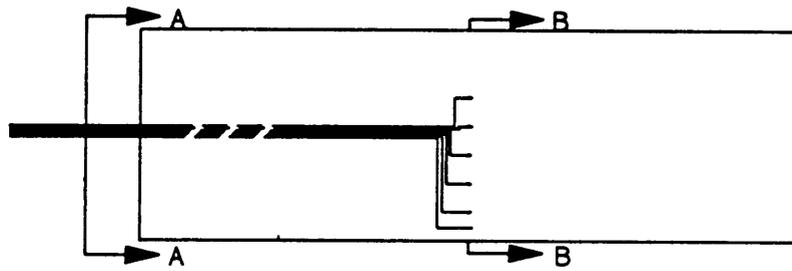
BOTTOM VIEW
BLADE 8

VIEW A-A

SECTION B-B
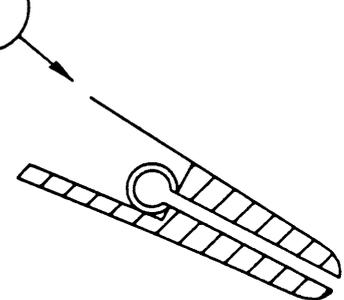
DETAIL I
(TYPICAL)

Figure 11.   Detail of the Blade Surface Static Taps
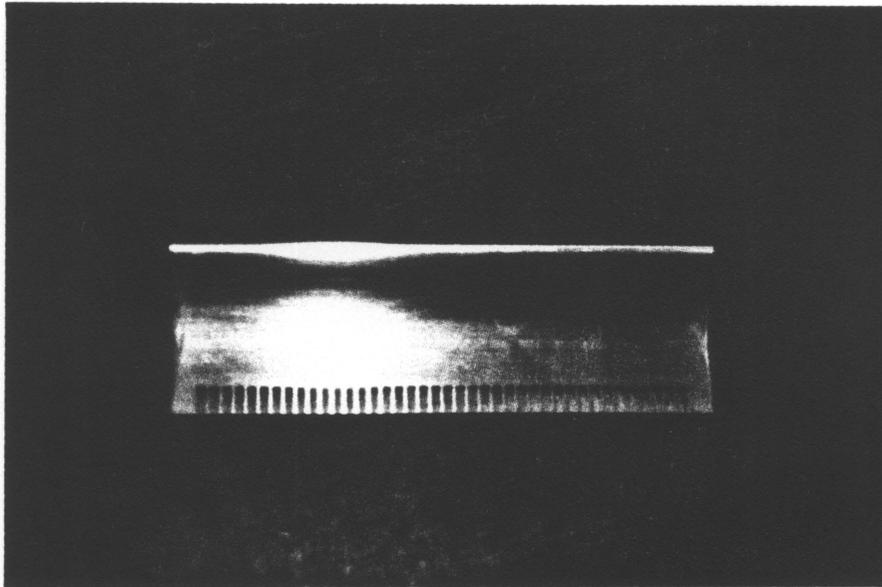
Figure 12. Cooled Blades: A photograph showing the pressure surface of one of the three cooled blades. Note the cooling holes at the trailing edge.
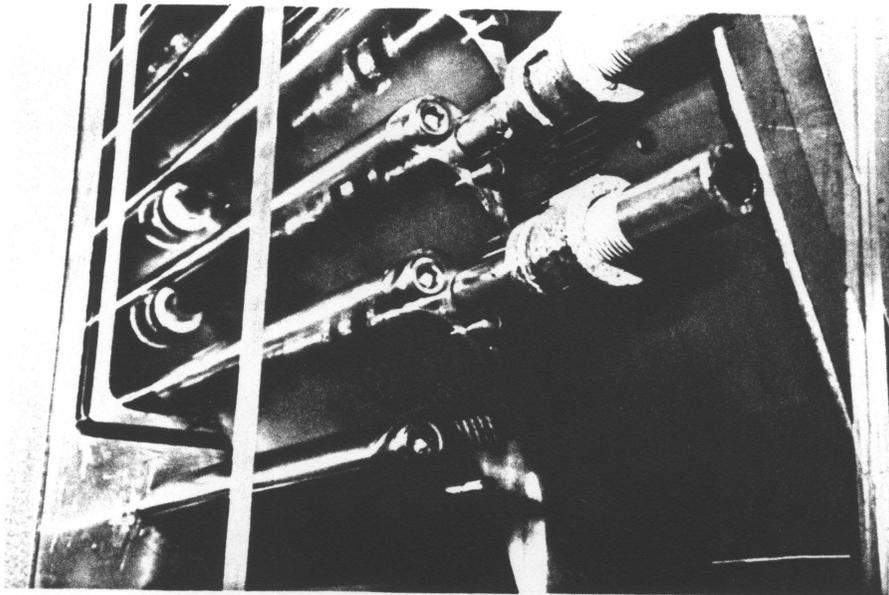
Figure 13. Coolant Supply System Fittings: A photograph showing special fittings which are inserted into the ends of the cooled blades through which CO_2 flows.
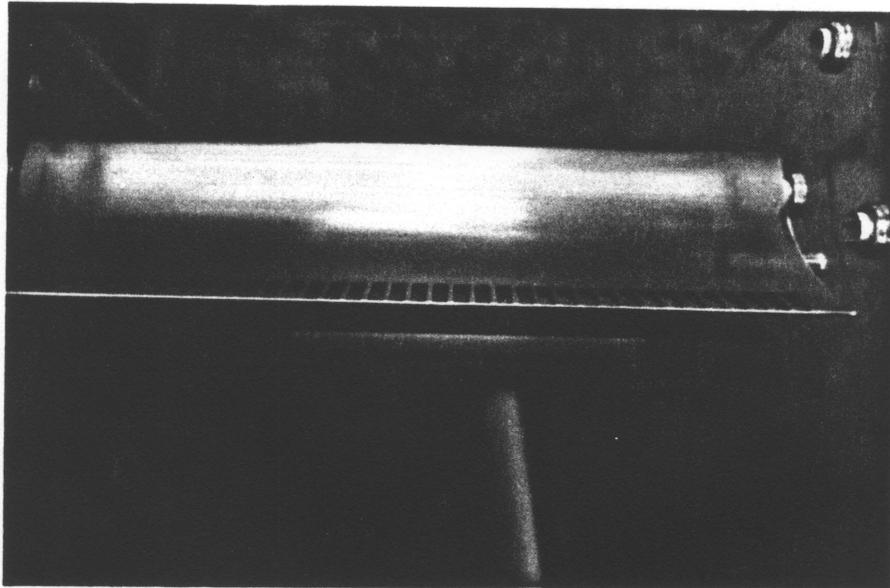
Figure 14. Coolant Injection Holes: A photograph showing the holes in the trailing edge of blades 4, 5 and 6 through which CO_2 is injected into the main flow.
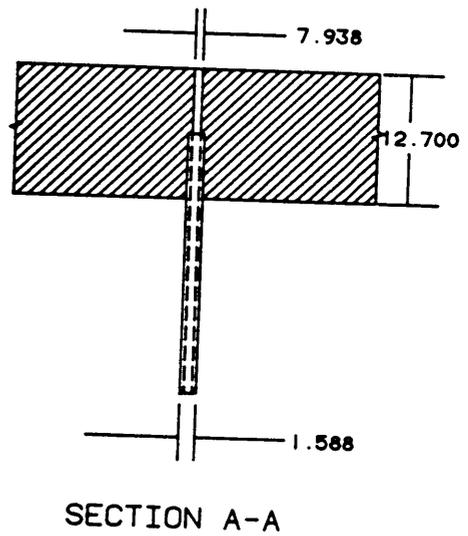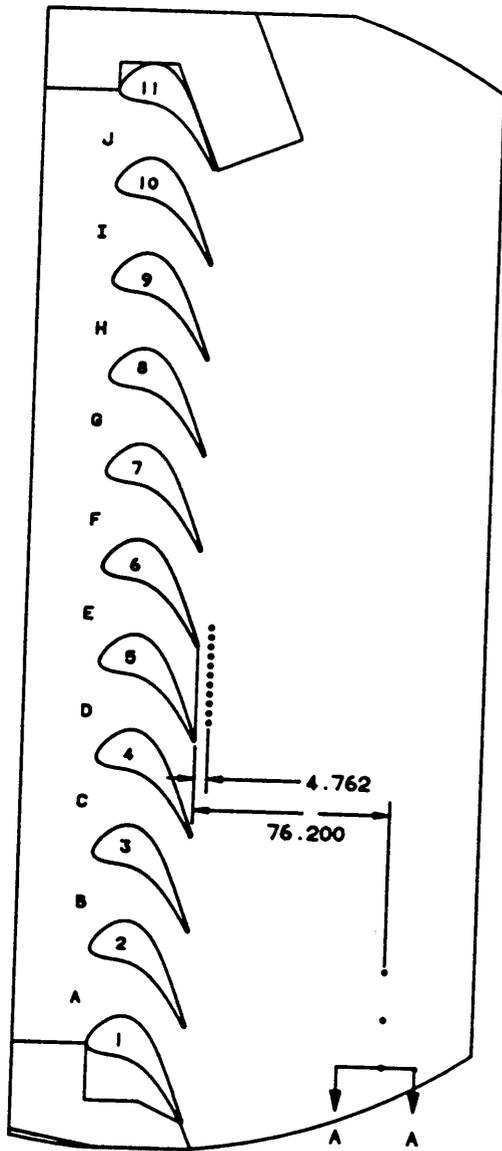
NOTE: ALL DIMENSIONS IN MM

Figure 15. Cascade Wall Static Pressure Taps
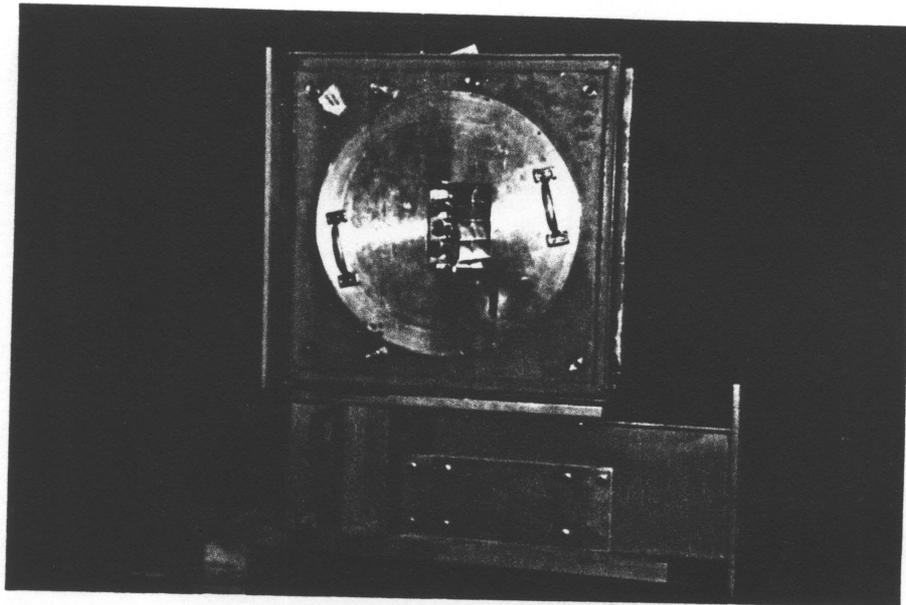
Figure 16. Test Section Doors: A photograph showing the right hand door of the test section. Note the 10.8 x 15.24 cm window through which several blade passages are visible.
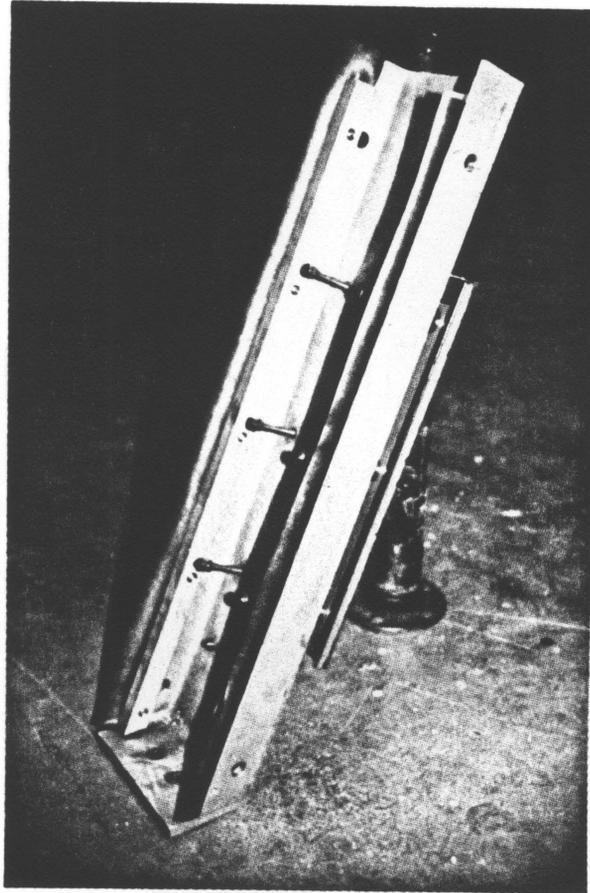
Figure 17. Test Section Back Wall: A photograph showing the back wall of the test section with the moveable tailboard attached. The tailboard adjusting bolts are also visible.
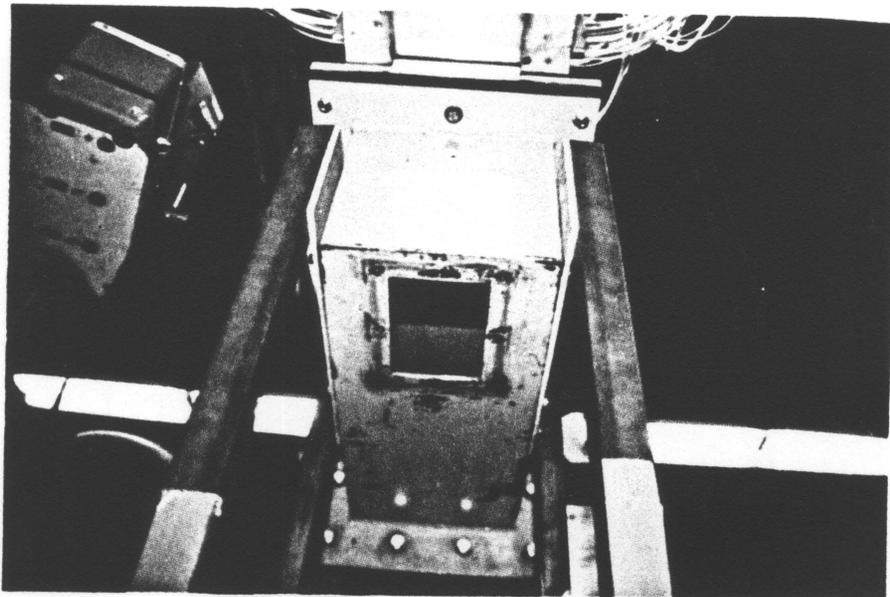
Figure 18. Probe Support Fixture Access Hole: A photograph showing the access hole in the bottom of the test section through which the total pressure probe support fixture is inserted.
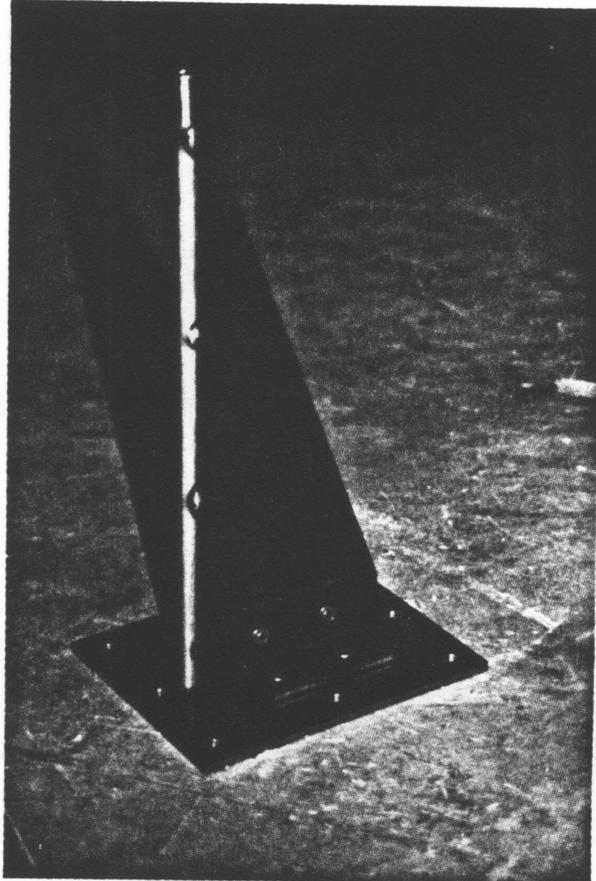
Figure 19. Probe Support Fixture: A photograph showing a fixture which provides support for the probe which measures the total pressure downstream of the blade row. A different fixture is used for each horizontal measurement location.
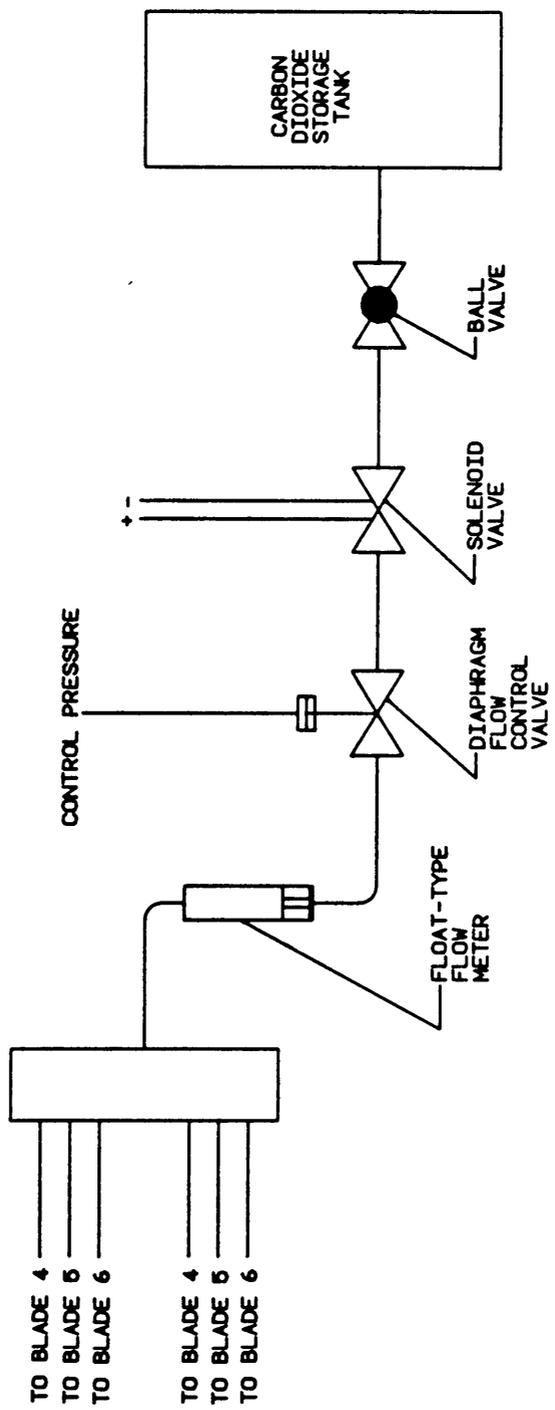
Figure 20. Coolant Supply System Schematic
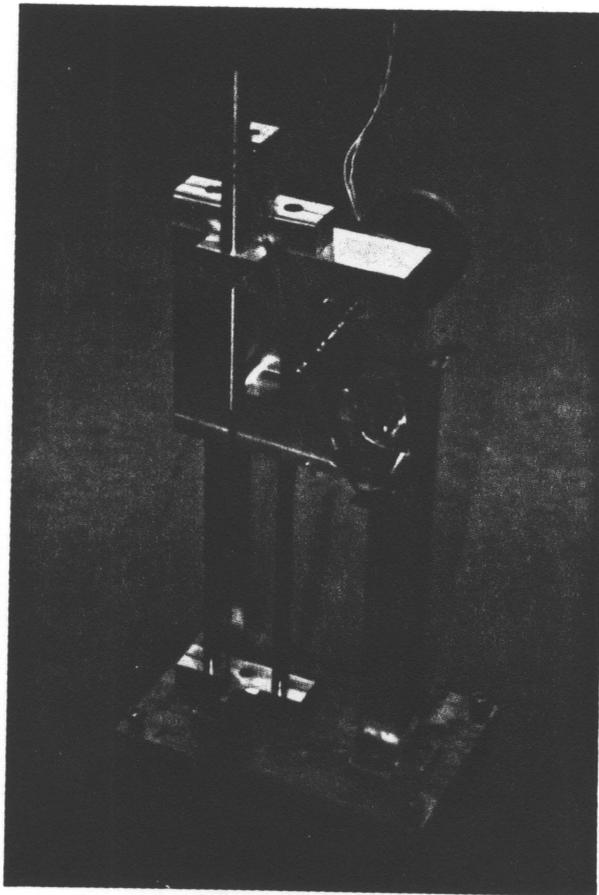
Figure 21. Total Pressure Probe Traversing Mechanism: A photograph showing the mechanism which drives the downstream total pressure probe.

CONCAVE MIRROR

PARTIALLY FOCUSSING
MIRROR

SHORT DURATION
LIGHT SOURCE

PARALLEL LIGHT

TEST SECTION

PLANE MIRROR

CAMERA

CONCAVE MIRROR
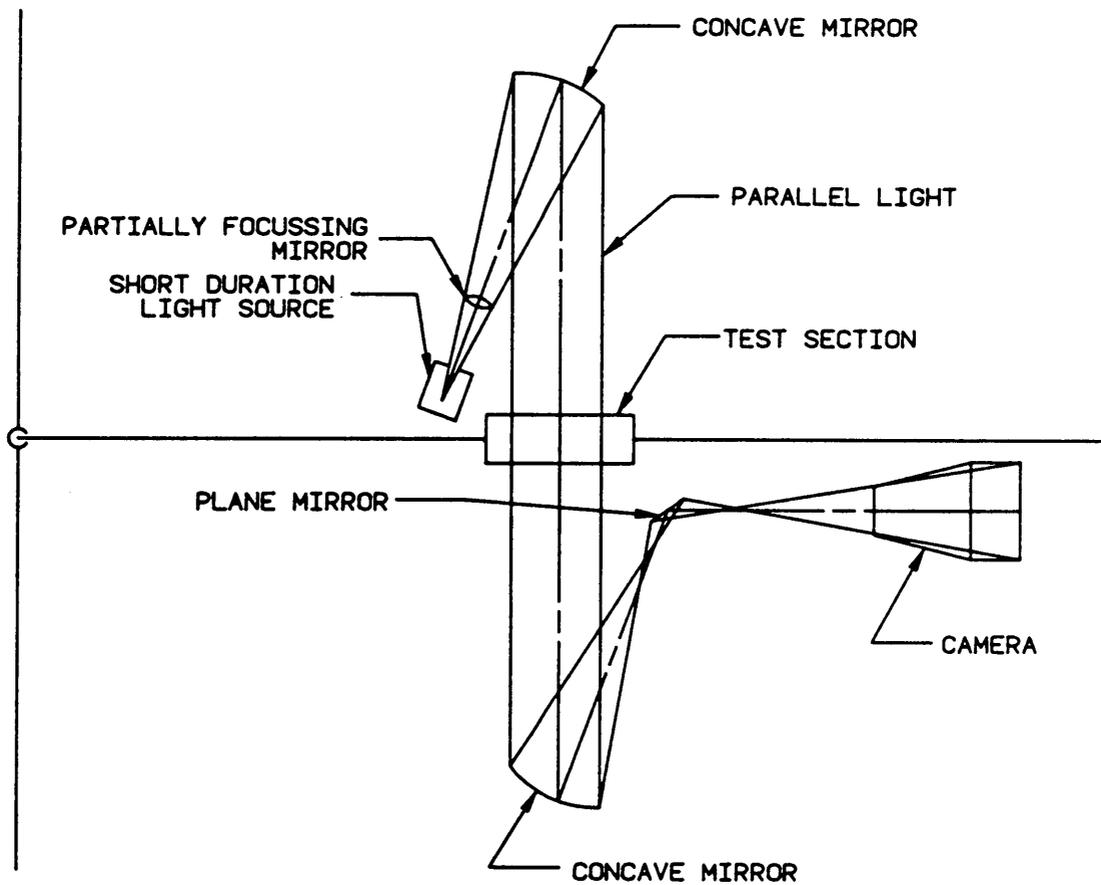
Figure 22.   Shadowgraph System Schematic

Figure 23. Typical Shadowgraph: Note the double reflection of an oblique shock off of the suction surface of the middle blade. Also note the shock reflection running from top right to bottom center. The silhouettes in the center of the picture are caused by the cascade wall static taps.

X/C=0.000   LEADING EDGE

X/C=1.000   TRAILING EDGE

X/C=1.125   FORWARD POSITION

X/C=1.667   MIDDLE POSITION

X/C=3.000   REAR POSITION
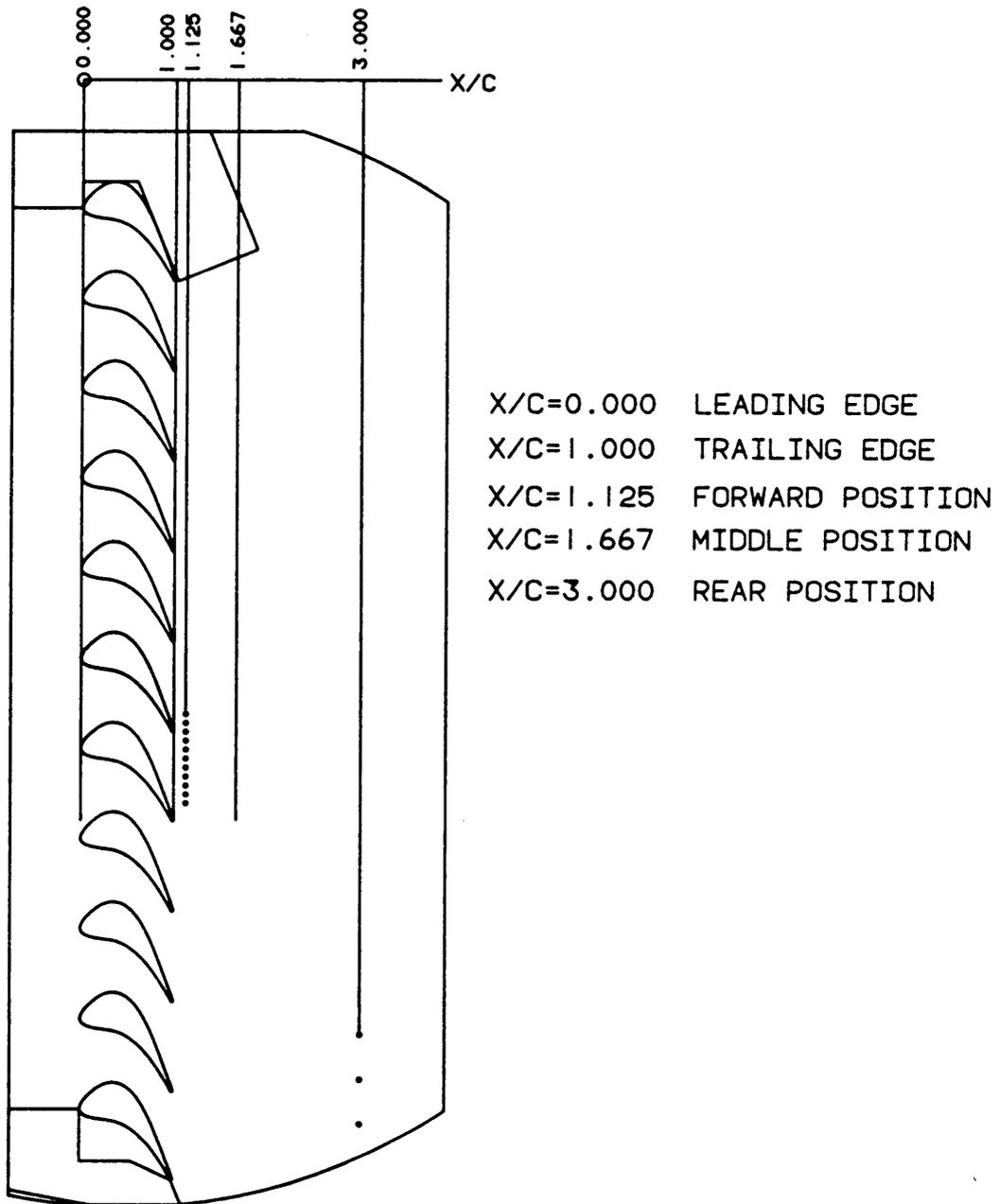
Figure 24.   Horizontal Measurement Locations
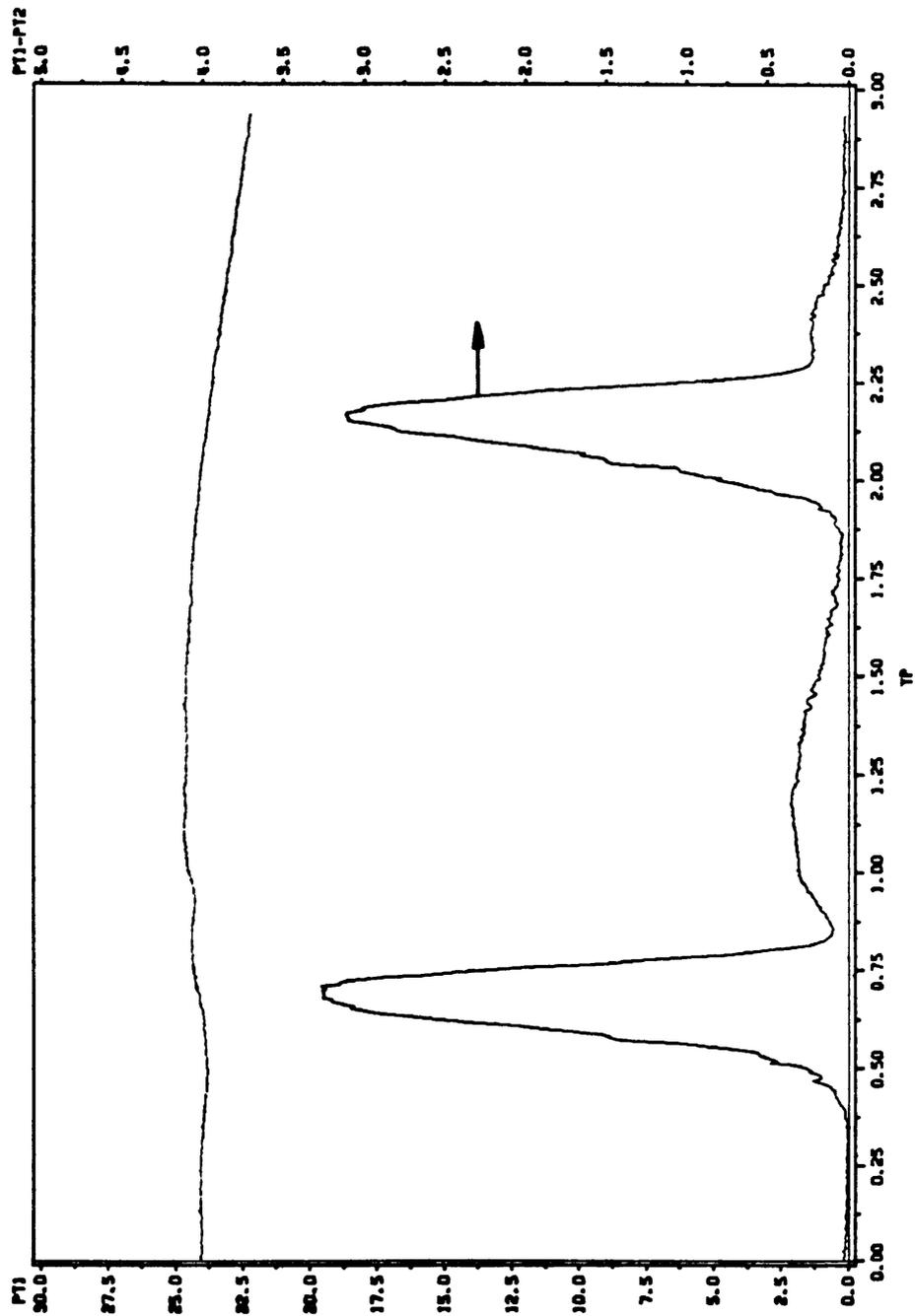
Figure 25. Typical Raw Data: $p_{t,1}$ and Δp_t vs. probe position, y_p, data taken at forward measurement location.
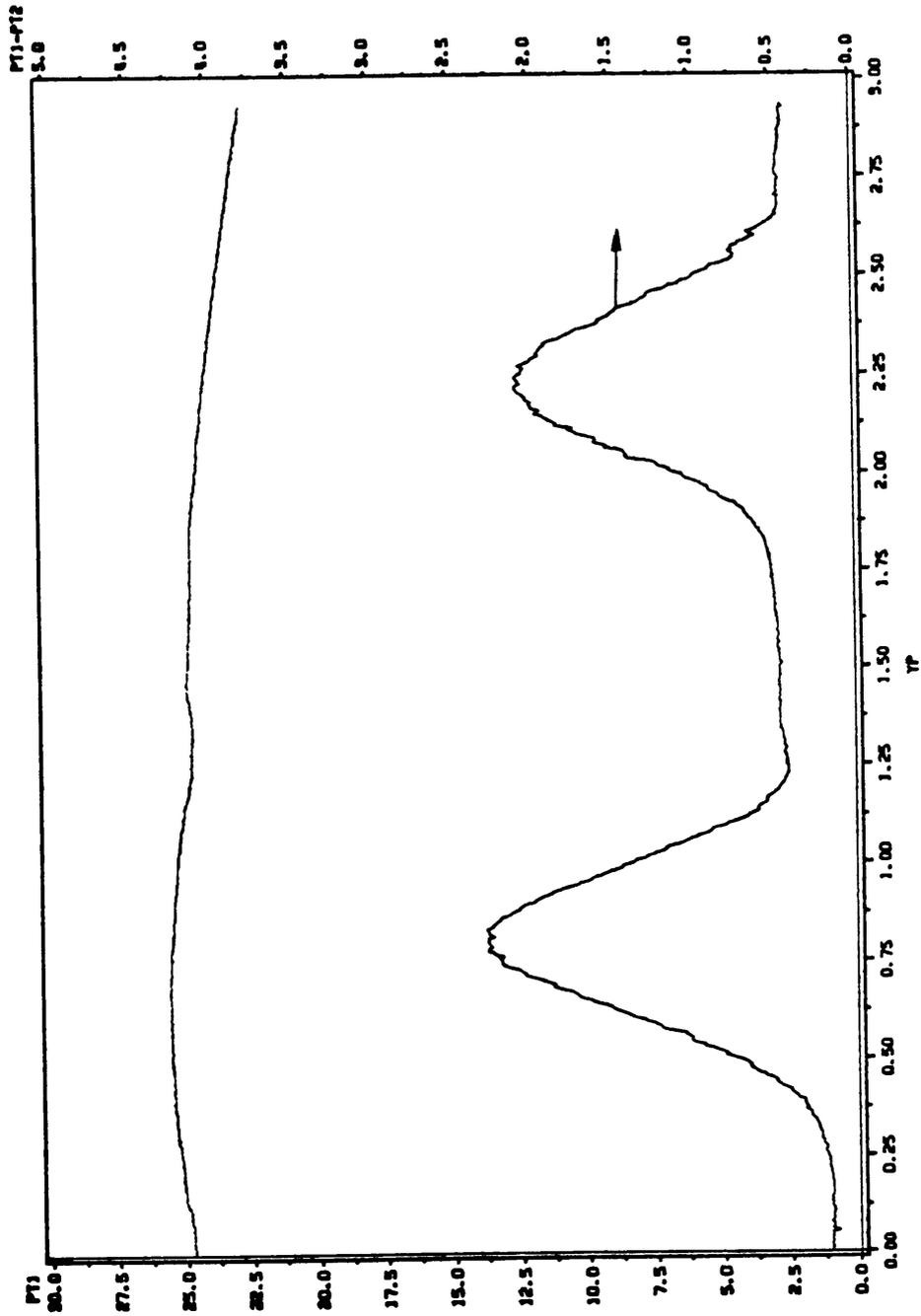
Figure 26. Typical Raw Data: $P_{t,1}$ and ΔP_t vs. probe position, y_p, data taken at middle measurement location.
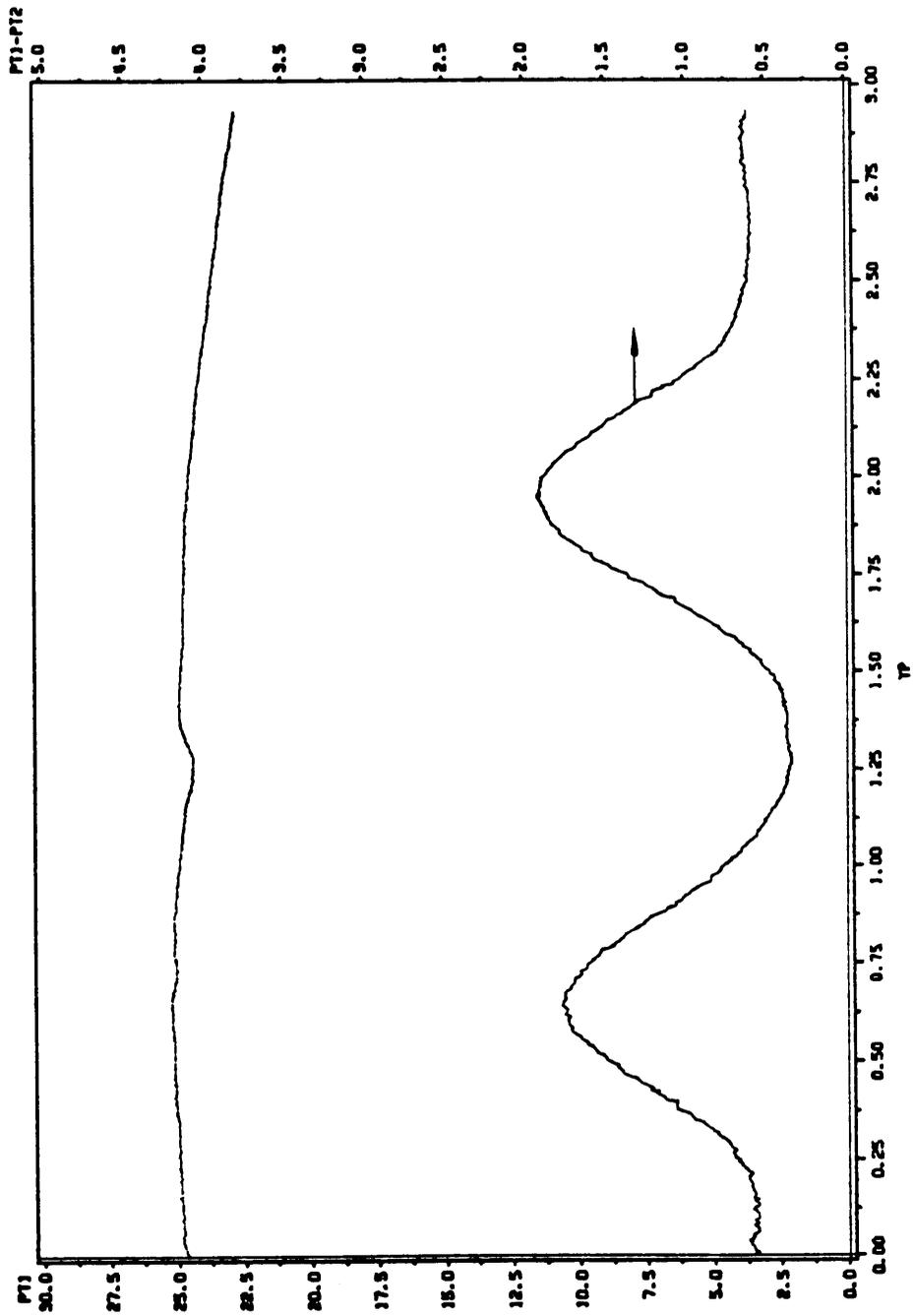
Figure 27. Typical Raw Data: $p_{t,1}$ and Δp_t vs. probe position, y_p, data taken at rear measurement location.
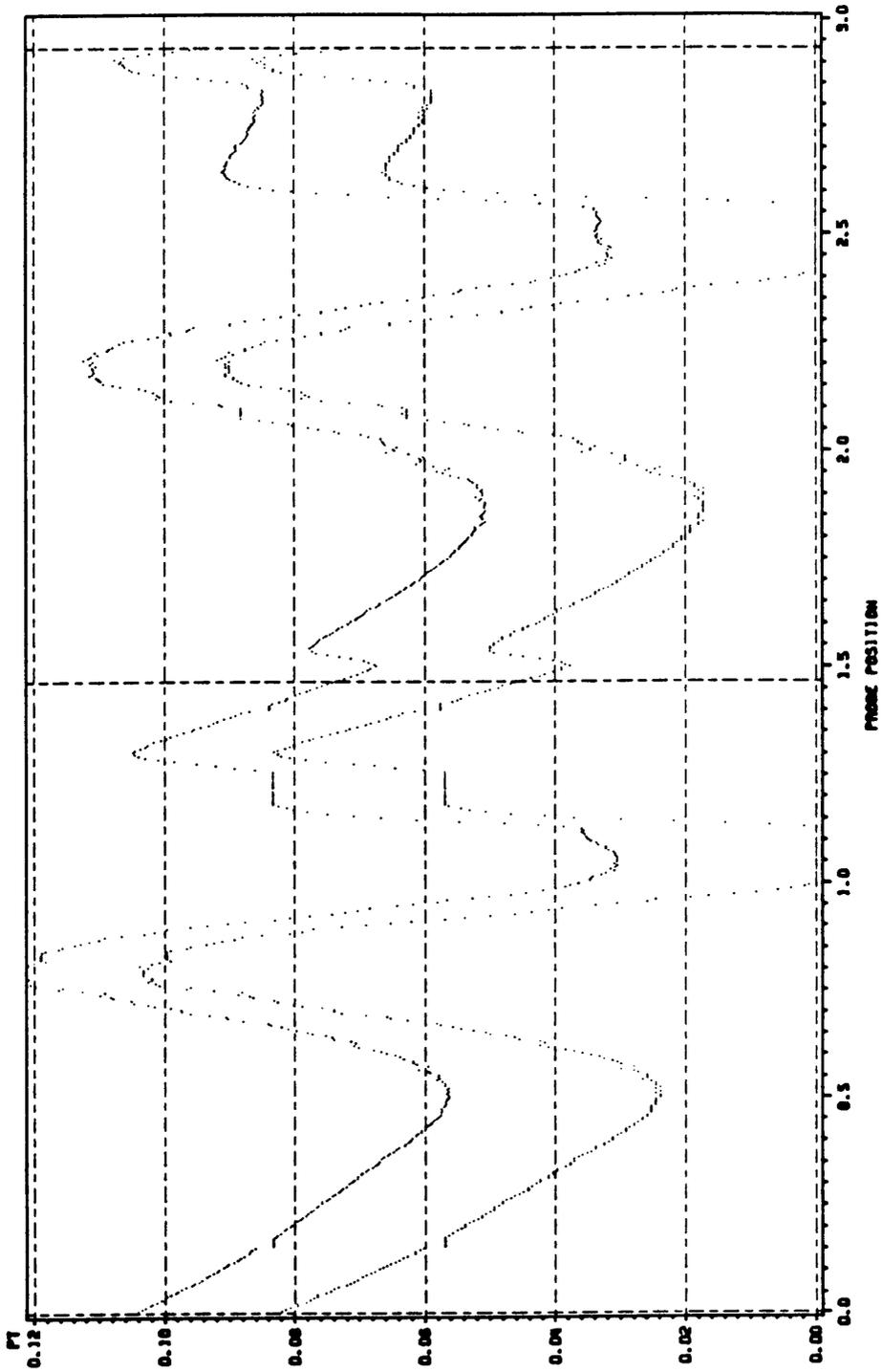
Figure 28. **Effect of Bow Shock Correction:** Shown are plots of P_t vs. y_p both with and without bow shock correction for the same data set. The top plot is for uncorrected data, the bottom plot is for data which is corrected for the probe tip bow shock.
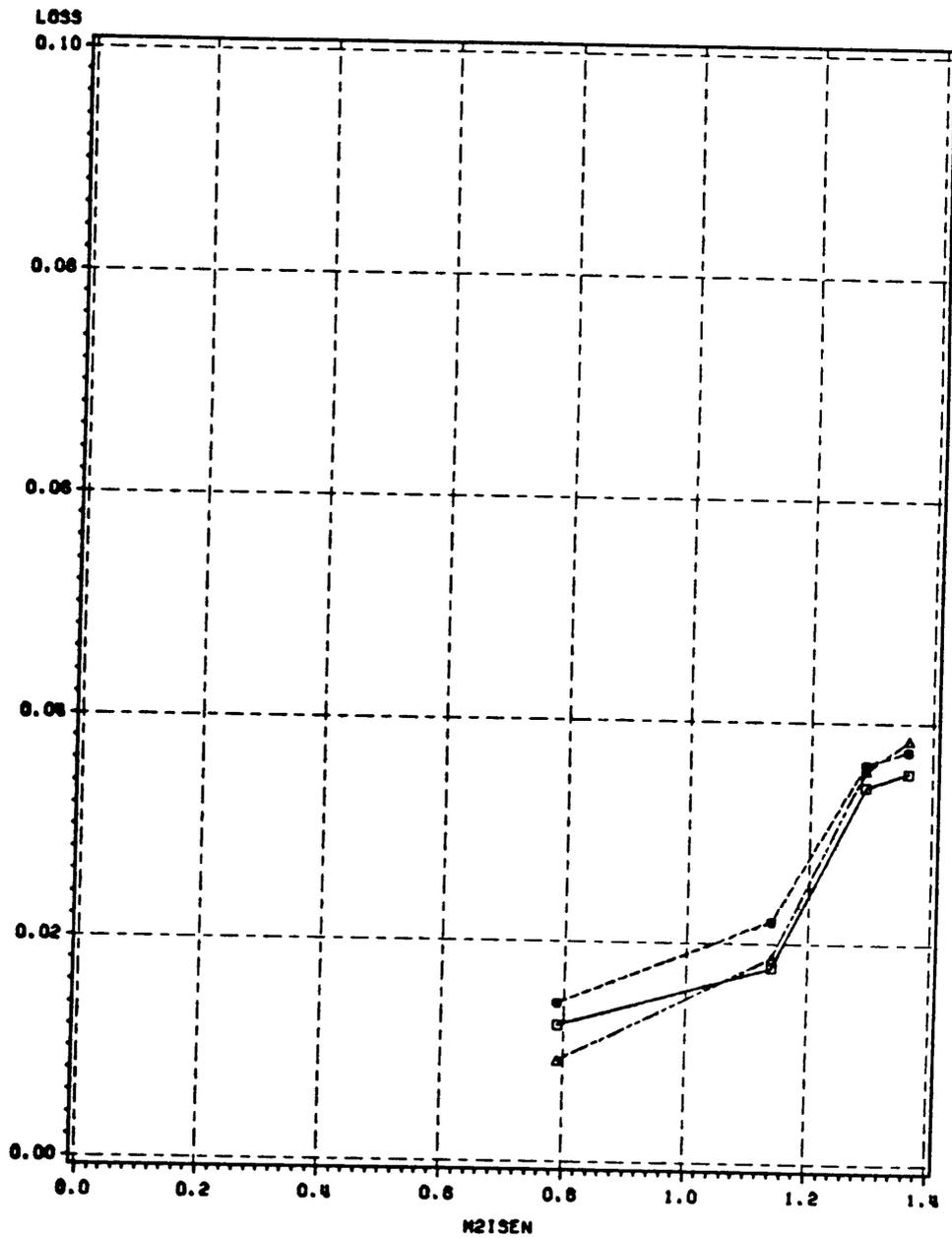
Figure 29. Loss vs. Blade Row Exit Average Isentropic Mach Number: $\frac{x}{c} = 1.125$ B:□-0
○-0.27 △-0.54
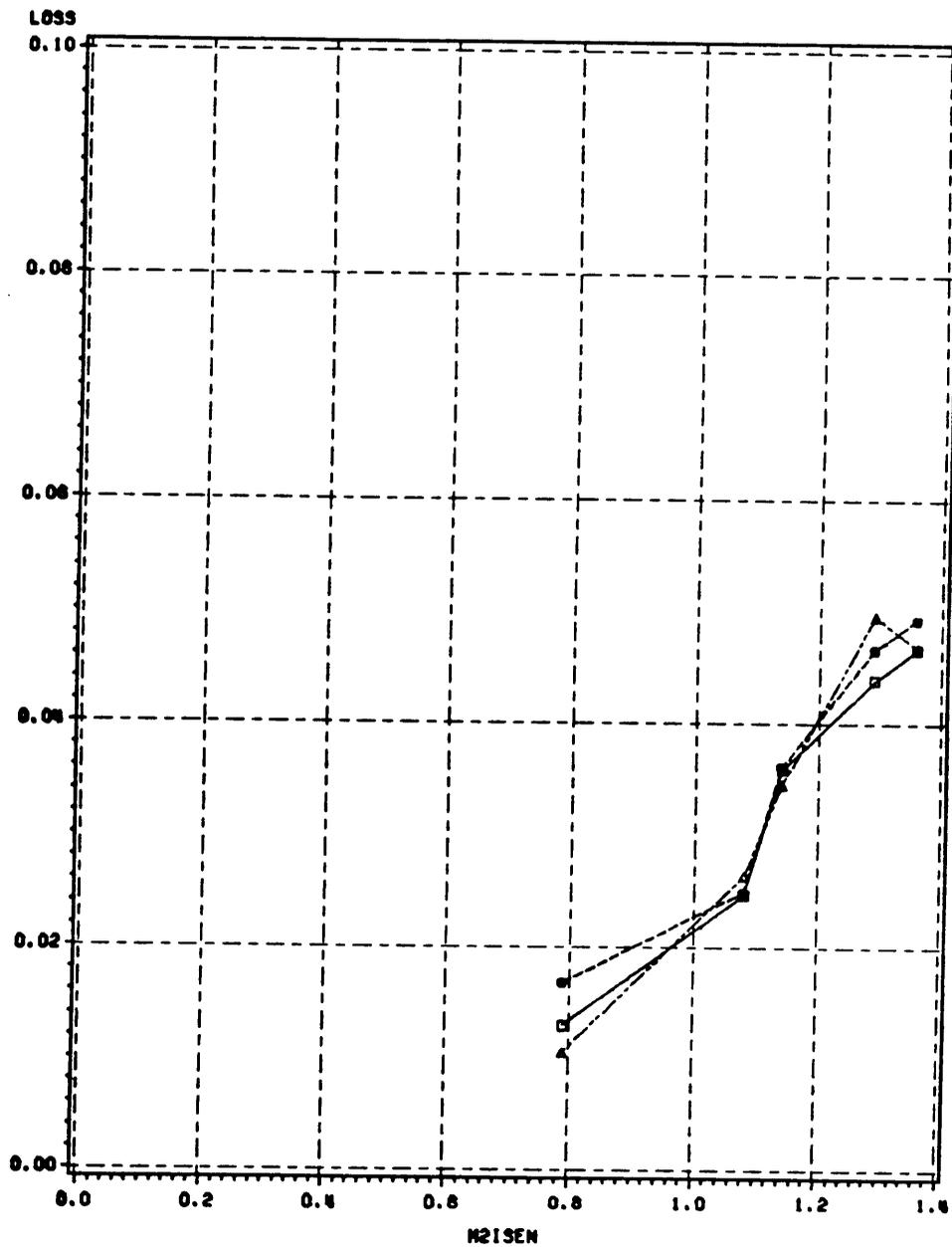
Figure 30. **Loss vs. Blade Row Exit Average Isentropic Mach Number:** $\frac{x}{c} = 1.667$ B:□-0 ○-0.27 △-0.54
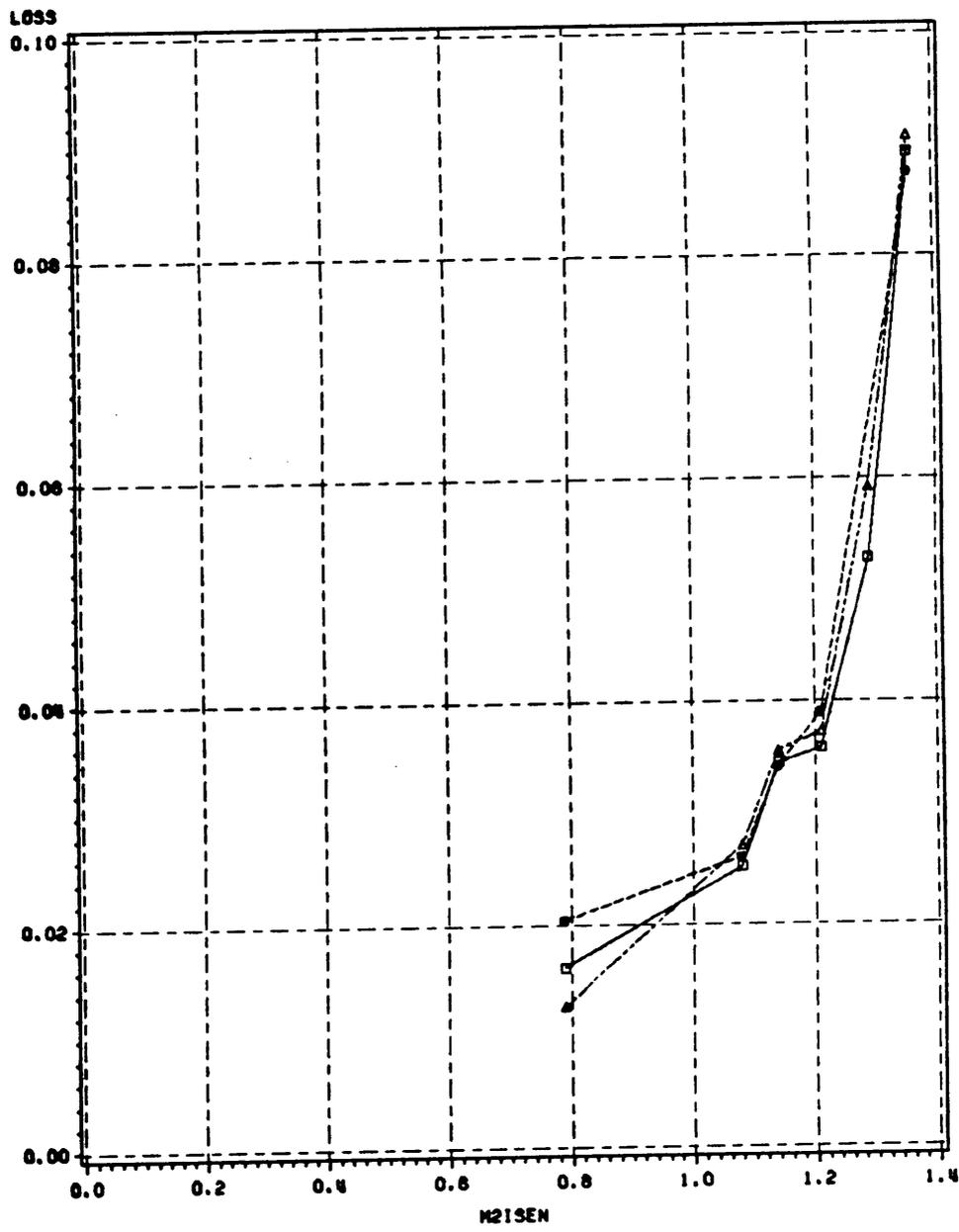
Figure 31. Loss vs. Blade Row Exit Average Isentropic Mach Number: $\frac{x}{c} = 3$ B: □-0 ○-0.27
△-0.54
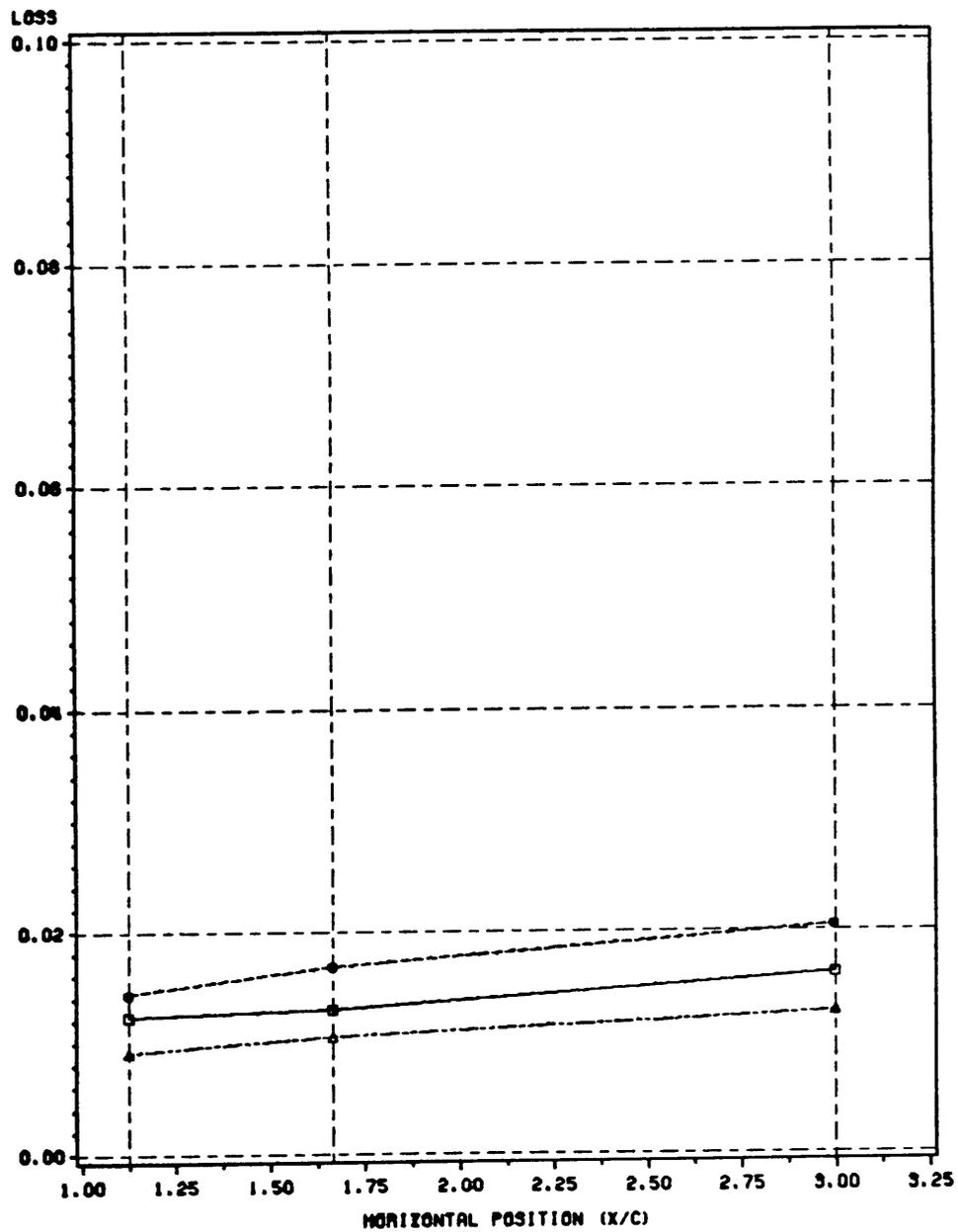
Figure 32. Loss vs. Horizontal Measurement Location: $M_{2,isen,avg} = 0.79$ B:□-0 ○-0.27 △-0.54
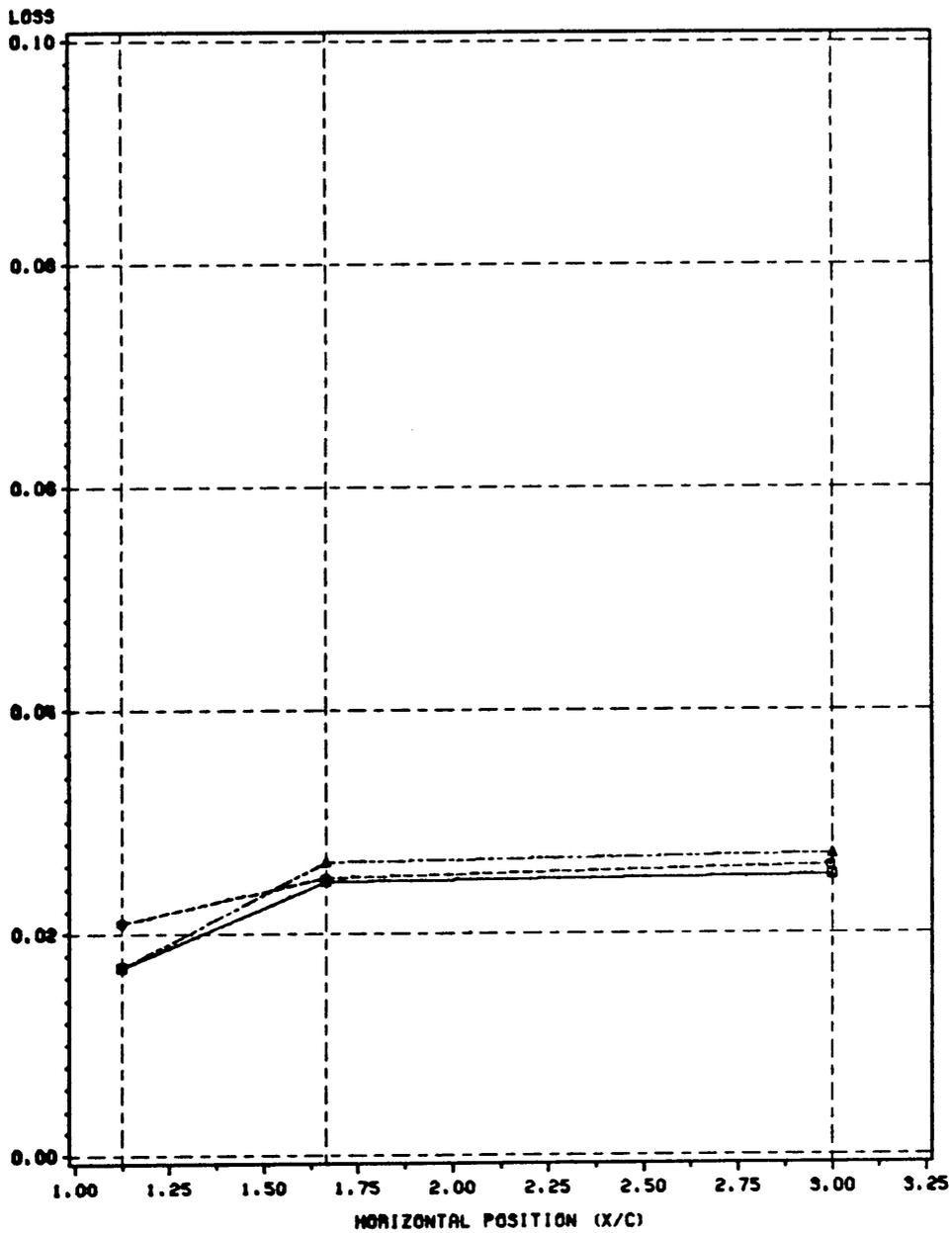
Figure 33. Loss vs. Horizontal Measurement Location: $M_{2,isen,avg} = 1.08$ B:$\square$-0 $\bigcirc$-0.27 $\triangle$- 0.54. Note that data for $\frac{x}{c} = 1.125$ was missing from the data set and was interpolated from Figure 29.
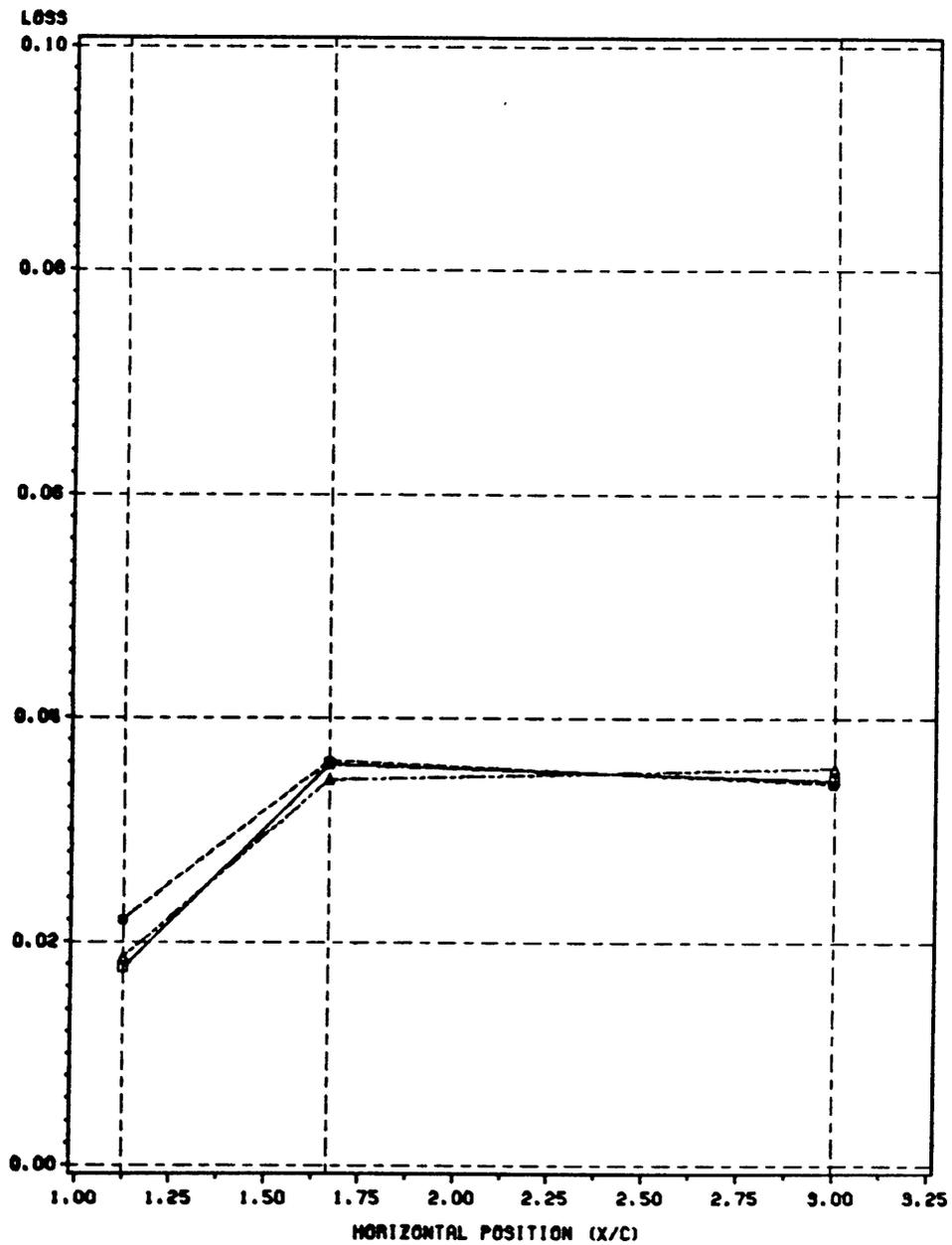
Figure 34. Loss vs. Horizontal Measurement Location: $M_{2,isen,avg} = 1.14$ B: □-0 ○-0.27 △-0.54.
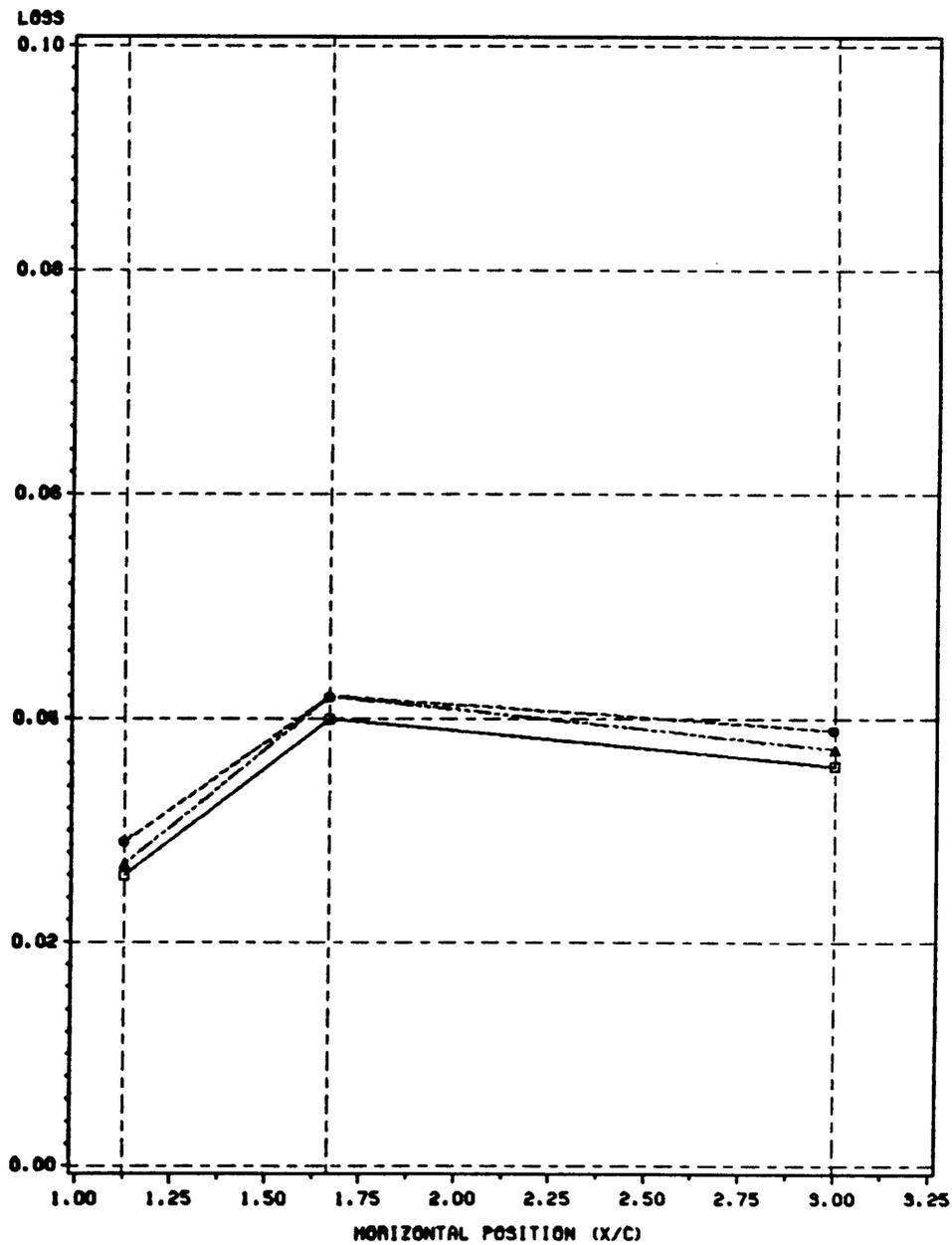
Figure 35. Loss vs. Horizontal Measurement Location: $M_{2,isen,avg} = 1.21$ B: □ -0 ○ -0.27 △ -0.54. Note that data for $\frac{x}{c} = 1.125$ and 1.667 was missing from the data set and were interpolated from Figure 29 and Figure 30.
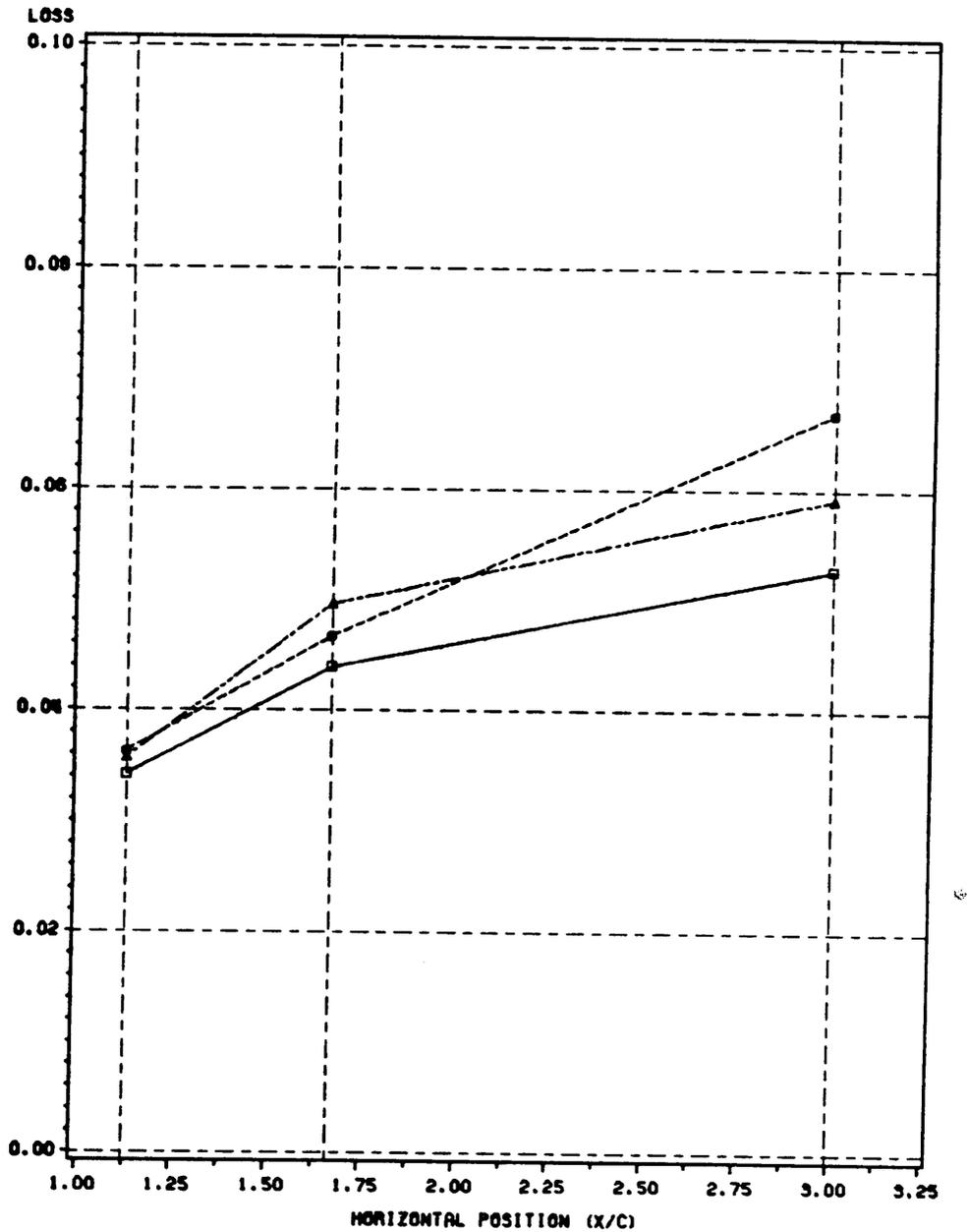
Figure 36. Loss vs. Horizontal Measurement Location: $M_{2,isen,avg} = 1.29$ B: $\square$-0 $\bigcirc$-0.27 $\triangle$-0.54. Note that data for $\frac{x}{c} = 3$, B $= 0.27$ was missing from the data setand were interploated from Figure 31.
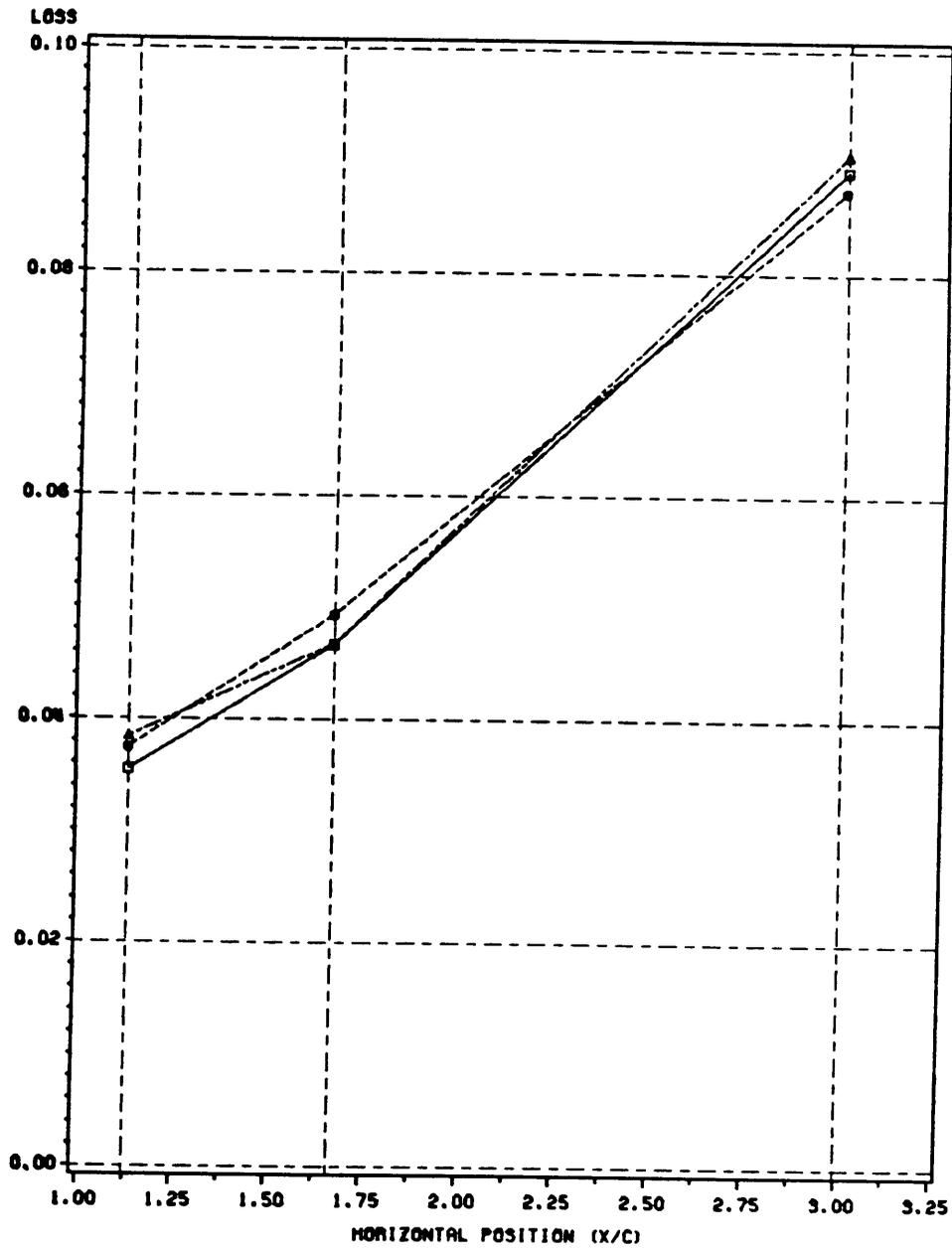
Figure 37.   Loss vs. Horizontal Measurement Location: $M_{2,isen,avg} = 1.36$ B:□-0 ○-0.27 △- 0.54
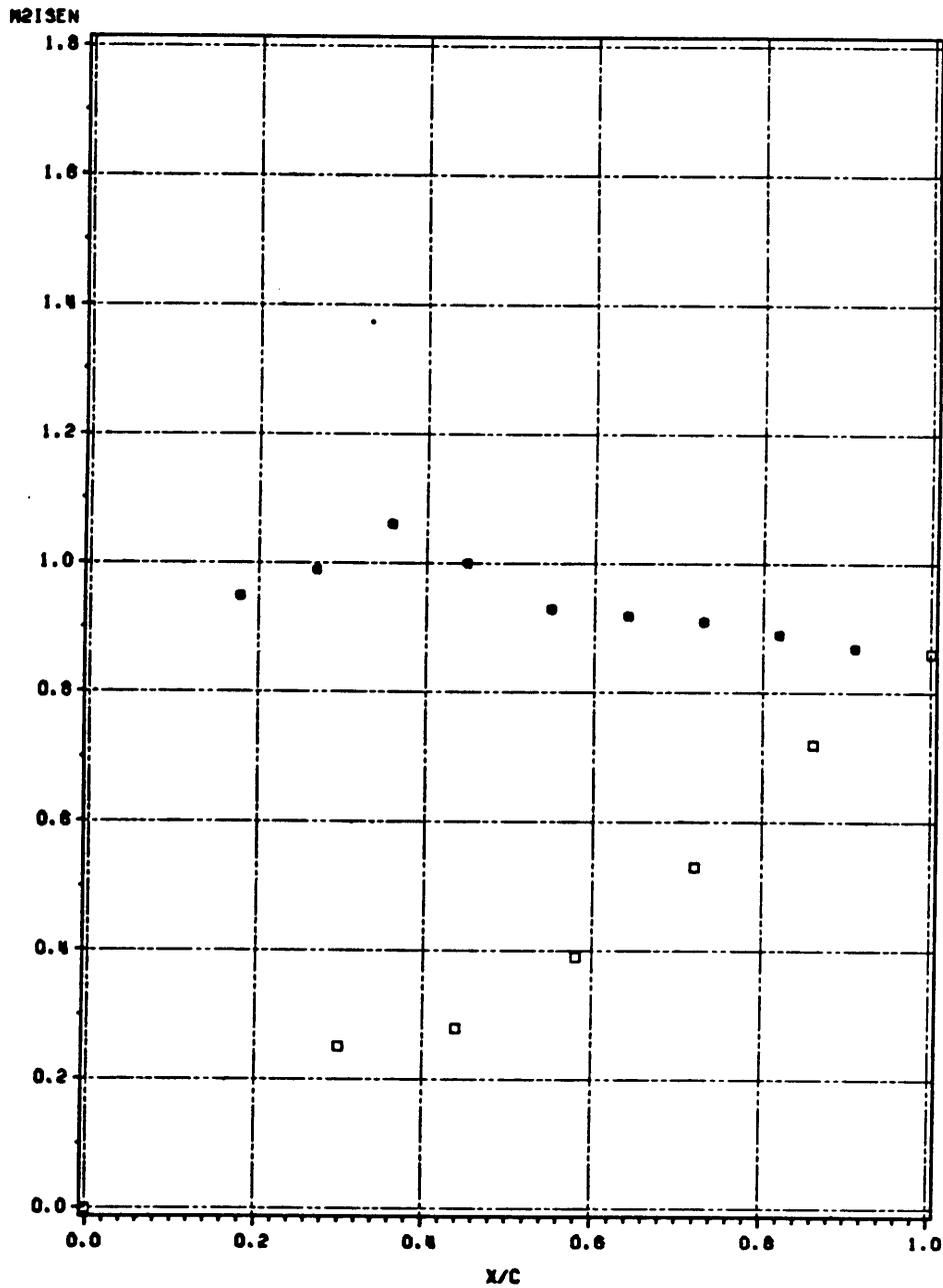
Figure 38. Blade Surface Pressure Distribution: $M_{2,isen,avg} = 0.79$ □-pressure surface ○-suction surface
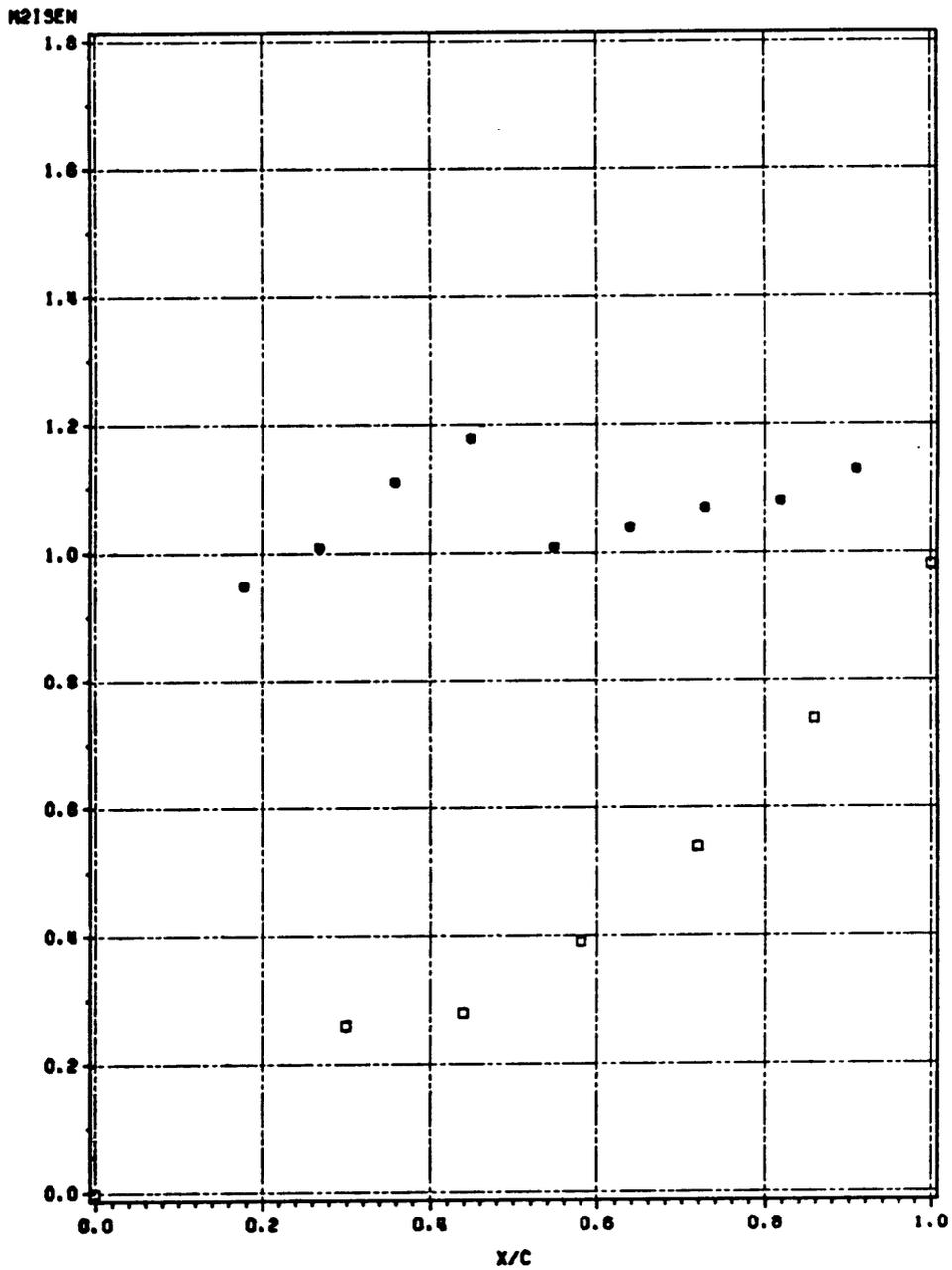
Figure 39. Blade Surface Pressure Distribution: $M_{2,isen,avg} = 1.08$ □-pressure surface ○-suction surface
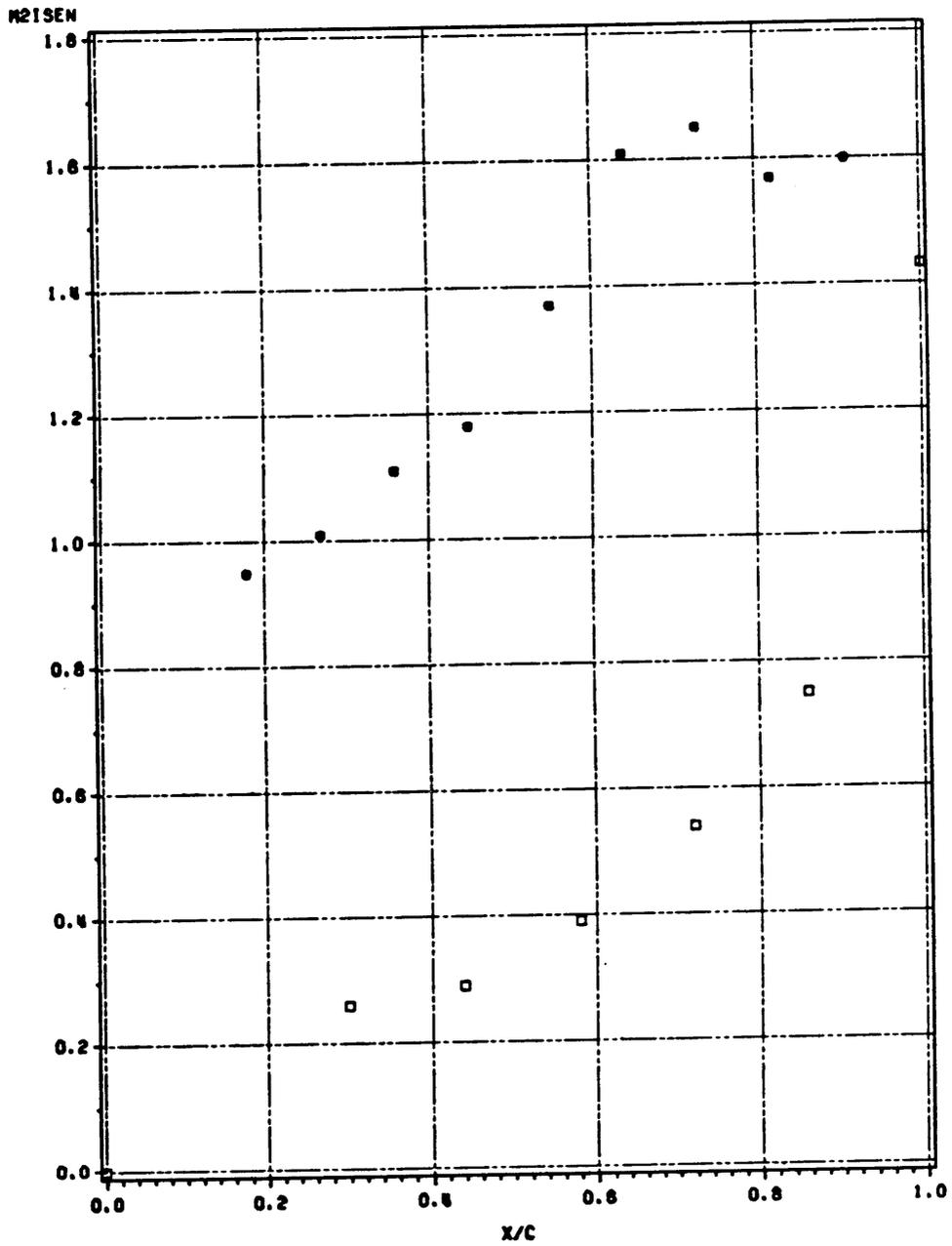
Figure 40. Blade Surface Pressure Distribution: $M_{2,isen,avg} = 1.36$ □-pressure surface ○-suction surface
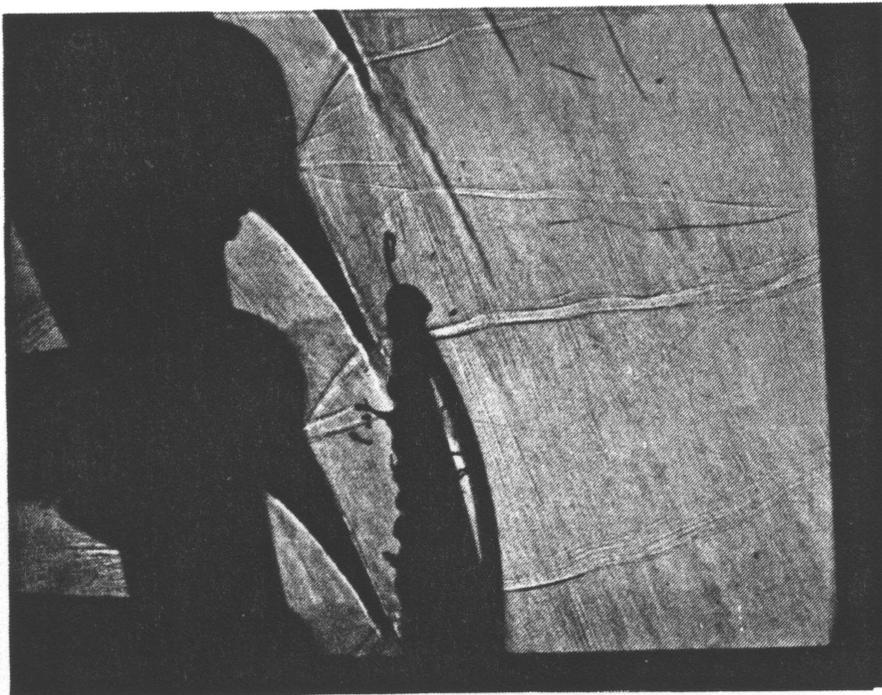
Figure 41. Trailing Edge Shock Stucture: $M_{2,isen,avg} = 1.08$ At top $B = 0$, at bottom $B = 0.54$
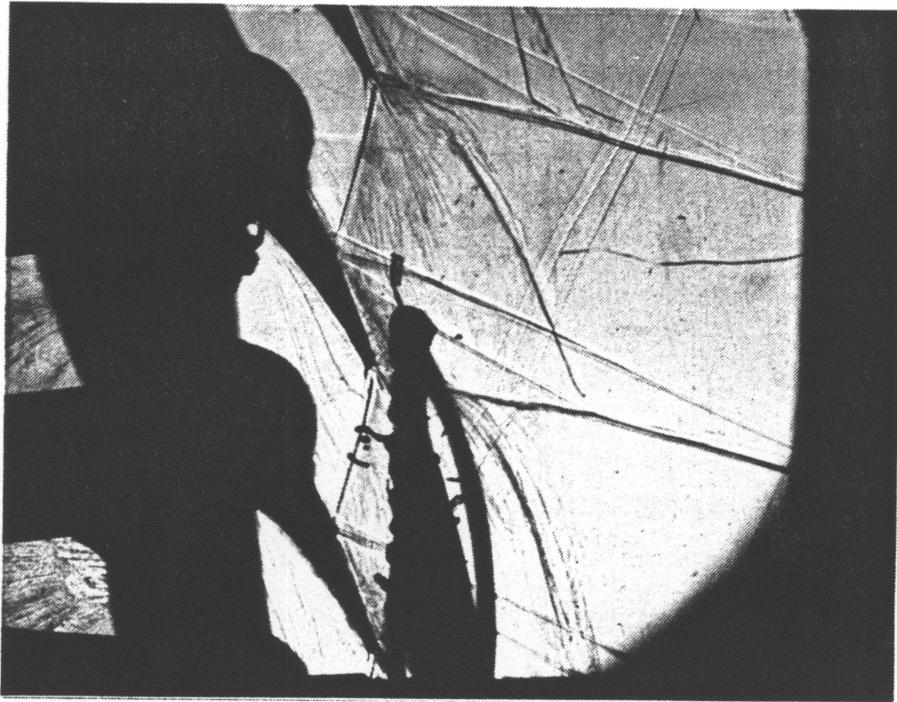
Figure 42.   Trailing Edge Shock Stucture: $M_{2,isen,avg} = 1.36$ At top B = 0, at bottom B = 0.54

Appendix B. Tables

**Table 1. Test Program**

(x/c)	B	M2,isen	M2,isen,avg	L
1.125	0	0.747	0.79	0.0124
1.125	0.27	0.796	0.79	0.0145
1.125	0.54	0.783	0.79	0.0092
1.667	0	0.756	0.79	0.0130
1.667	0.27	0.774	0.79	0.0169
1.667	0.54	0.780	0.79	0.0106
3.000	0	0.815	0.79	0.0162
3.000	0.27	0.828	0.79	0.0205
3.000	0.54	0.842	0.79	0.0127
1.125	0	——	——	——
1.125	0.27	——	——	——
1.125	0.54	——	——	——
1.667	0	1.081	1.08	0.0247
1.667	0.27	1.079	1.08	0.0250
1.667	0.54	1.076	1.08	0.0264
3.000	0	1.076	1.08	0.0252
3.000	0.27	1.068	1.08	0.0261
3.000	0.54	1.071	1.08	0.0271

——Data not available

Table 2. Test Program (cont'd)

(x/c)	B	M2,isen	M2,isen,avg	L
1.125	0	1.156	1.14	0.0178
1.125	0.27	1.144	1.14	0.0221
1.125	0.54	1.155	1.14	0.0187
1.667	0	1.117	1.14	0.0359
1.667	0.27	1.138	1.14	0.0362
1.667	0.54	1.139	1.14	0.0345
3.000	0	1.158	1.14	0.0345
3.000	0.27	1.143	1.14	0.0342
3.000	0.54	——	——	——
1.125	0	——	——	——
1.125	0.27	——	——	——
1.125	0.54	——	——	——
1.667	0	——	——	——
1.667	0.27	——	——	——
1.667	0.54	——	——	——
3.000	0	1.213	1.21	0.0358
3.000	0.27	1.213	1.21	0.0390
3.000	0.54	1.212	1.21	0.0373

——Data not available

Table 3. Test Program (cont'd)

(x/c)	B	M2,isen	M2,isen,avg	L
1.125	0	1.298	1.29	0.0342
1.125	0.27	1.297	1.29	0.0363
1.125	0.54	1.293	1.29	0.0357
1.667	0	1.293	1.29	0.0439
1.667	0.27	1.291	1.29	0.0467
1.667	0.54	1.288	1.29	0.0496
3.000	0	1.288	1.29	0.0528
3.000	0.27	——	——	——
3.000	0.54	1.294	1.29	0.0592
1.125	0	1.368	1.36	0.0355
1.125	0.27	1.366	1.36	0.0375
1.125	0.54	1.363	1.36	0.0385
1.667	0	1.365	1.36	0.0467
1.667	0.27	1.361	1.36	0.0494
1.667	0.54	1.359	1.36	0.0468
3.000	0	1.356	1.36	0.0893
3.000	0.27	1.352	1.36	0.0875
3.000	0.54	1.347	1.36	0.0907

——Data not available

The vita has been removed from
the scanned document